This is to certify that the

thesis entitled

Transverse permeation and compaction of stacks of random, continuous glass fiber mats

presented by

Sanjay Mishra

has been accepted towards fulfillment of the requirements for

MS degree in Chemical Engineering

Dr. K. Jayaraman
Major professor

Date August 6, 1993

TRANSVERSE PERMEATION AND COMPACTION OF STACKS OF RANDOM, CONTINUOUS GLASS FIBER MATS

By

Sanjay Mishra

A THESIS

Submitted to
Michigan State University
in partial fulfillment of the requirements
for the degree of

MASTER OF SCIENCE

Department of Chemical Engineering

1993

ABSTRACT

TRANSVERSE PERMEATION AND COMPACTION OF STACKS OF RANDOM, CONTINUOUS GLASS FIBER MATS

By

Sanjay Mishra

The effect of fiber volume fraction and compaction on the transverse permeability of a fluid flowing through stacked layers of fiber mats has been studied. Random mats of continuous strands were pressed at different loads to prepare preforms. Mixtures of glycerol and water (various viscosities) were used to simulate the resin.

An empirical equation was developed to relate the permeability to the fiber volume fraction. This relation was used with measurements in the nonlinear region of the flow rate - pressure drop curve, to infer the changing fiber volume fraction with varying pressure drop in any run. A model relating the effective stress carried by the fibers to the fiber volume fraction was developed and was used to predict the entire pressure drop - flow rate profile. Higher viscosity fluids led to a greater degree of compaction in flow through preforms, at the same pressure drop.

Dedicated to my parents, who have always taught me the essence of hard work in life.

ACKNOWLEDGEMENTS

I thank Dr. K. Jayaraman for his steadfast support, guidance and inspiration, but for which this work couldn't have been completed.

I deeply appreciate the help provided by Mike Rich and Brian Rook in the CMSC laboratory. Thanks are also due to the DER machine shop personnel, specially to Mike McLean for constructing the permeation cell.

I am indebted to Nancy, Satyadev, Brent and Venky, who provided me valuable suggestions throughout the course of this work. My friends and well-wishers deserve special credit for their support and encouragement. In particular I would like to thank Gunjan.

Finally, I acknowledge the teachings and emotional support provided by my parents, who, although so far from me, have always prayed for my success.

TABLE OF CONTENTS

LIST OF TABLES

LIST OF FIGURES

NOMENCLATURE

a	Fitting constant in equations (3.5) and (3.6), m^2
A	Fitting constant in equation (3.3), m^2
A, A_f	Cross-sectional area of preform, m^2
b	Exponent in equation (3.6)
B	Orientation constant in equation (3.3)
c	Constant used in equation (2.2), m
d	Diameter of fiber, m
d_f	Filament diameter, m
E	Young's modulus of fiber, N/m^2
g	Gravitational constant, m/s^2
H	Height of fiber bundle, m
I	Moment of inertia, m^4
k_{zz}	Kozeny constant
K	Permeability, m^2
K_h	Hydraulic constant
K_{ii}	In-plane permeability, m^2
K_{zz}	Transverse permeability, m^2
L	Average span length of fiber, m
m	Mass of wicking liquid at any time t in equation (2.2), kg
	Slope of linear region in equation (4.3), $m^3/Pa\text{-}s$
m_f	Mass of preform, kg
n	Exponent in equation (3.5)
P_a	Applied pressure on preform, Pa
P_r	Average resin pressure, Pa
ΔP	Pressure drop across preform thickness, Pa
ΔP_c	Critical pressure drop, Pa
Q	Flow rate, m^3/s
Q_c	Critical flow rate, m^3/s
r_f	Tow radius, m
s	Constant used in equation (4.10)
t_a	Minimum possible thickness of preform, m
t_i,t	Thicknesses of preform at fiber volume fractions V_i and V_f respectively, m
t	Time in equation (2.2), s
t_f	Thickness of preform,m

V_f Fiber volume fraction of preform
V_i, V_{ini} Initial fiber volume fraction of preform
V_m, V_{max} Maximum possible fiber volume fraction of preform
V_T Total volume occupied by fiber bundle, m^3
V_{ah} Maximum possible fiber volume fraction of a preform consisting of hexagonal arrays
w_b Weight fraction of binder in preform
W_f Weight of fiber bundle, kg
Y Deflection of fiber due to load σ, m

Greek symbols

α Slope of m vs t on a log-log plot (equation 2.2)
Square root of V_f/V_m in equation (3.2)
γ_l Surface tension of wicking liquid, N/m
$\Delta\gamma$ Difference in surface free energy between a unit area of dry surface & a unit area of wetted surface, N/m
ϵ Porosity in fiber bundle
θ Contact angle between fiber and liquid surface, degrees
μ Viscosity of liquid, Pa-s
ρ_f Density of E-glass fibers, kg/m^3
ρ_l Density of wicking liquid, kg/m^3
σ Effective stress carried by fibers at any V_f, Pa
σ_i Initial effective stress, Pa

Chapter 1 Introduction

This chapter enumerates the basic concepts associated with permeability measurements, discusses the need of undertaking transverse permeability studies and gives a brief outline of previous work done in this field.

1.1 Motivation

Liquid molding processes, e.g., SRIM, RTM, are popular methods for production of fiber reinforced composites. A composite is simply a combination of two materials, possessing properties that are superior to either of its components. In a liquid molding process, fibers of glass, carbon or aramid are packed in a mold of the desired shape. A resin (prepolymer) is then poured into the mold. After filling, polymerization is allowed to take place. When curing of the polymer is completed, the composite is demolded. In this process, the composite properties that are sought to be enhanced include the mechanical strength and surface quality, among others. The packing of fibers in a preform needs to be optimized to obtain the best properties. If the fibers are too densely packed, some part of the preform may not come into contact with the resin. Too loose a packing might result in the resin flowing around the fiber bundles without penetrating it. Both these extremes would result in decrease of mechanical strength of the final part.

The mold design, which involves fiber content as a parameter, therefore, plays a very important role in enhancement of the desired properties.

Though molding processes have been in operation for a fairly long time, it is surprising that not enough data exist for the proper optimization of the mold design. Therefore, it would be beneficial to understand more about the physical issues that affect the molding process. Study of the fluid mechanics of the resin filling the mold can help a lot in getting closer to an optimal mold design. This includes information about the pressure profile as function of resin viscosity, preform type (and quantity) and mold geometry.

For flow of resin through the thickness of a stack of fiber mats, it has been observed [9,10] that high flow rates result in compaction of the stack. This leads to changes in fiber volume fraction of the stack, thereby affecting its permeability. This phenomenon of compaction caused by the flow of resin, has not been quantified so far. For accurate permeability determination, the process of compaction needs to be investigated both qualitatively and quantitatively. The present work is an attempt to gain more knowledge in this area.

1.2 Fundamental concepts

A preform is made up of a number of layers of fiber mats, stacked on top of one another. This is the reinforcement in the final composite part. There exist many different classifications of the fiber mats : unidirectional - bidirectional, stitched - woven, random - aligned, etc. Detailed descriptions of these can be found in [1]. A preform may consist

of one or more type(s) of fiber mats. To prepare a preform, the fiber mats are heated so that the binder melts. These mats are then pressed into the shape of the desired object. Cooling re-solidifies the binder, thereby causing the reinforcement to retain its shape. Finally this preform is put in a different mold and resin is added to get the final composite.

Permeability is a measure of the ease with which the resin flows through the preform. It arises from Darcy's law, which can be written as:

$$\mu v = -K.\nabla P$$

μ is the viscosity of the fluid, v its superficial velocity, P is the pressure and K, a second order tensor, is the permeability. Mathematically it is represented as:

$$K_{ij} = \begin{bmatrix} K_{11} & K_{12} & K_{13} \\ K_{21} & K_{22} & K_{23} \\ K_{31} & K_{32} & K_{33} \end{bmatrix}$$

Here i is the flow direction and j is the permeability component. If the permeability is orthotropic, then $K_{21} = K_{12}$, $K_{31} = K_{13}$ and so on and there exists a principal coordinate system (x,y,z) such that

$$K_{ij} = \begin{bmatrix} K_{xx} & 0 & 0 \\ 0 & K_{yy} & 0 \\ 0 & 0 & K_{zz} \end{bmatrix}$$

The components K_{xx} and K_{yy} are also termed in-plane permeabilities. K_{zz} is called the transverse (or z) permeability or the permeability in the thickness direction.

Fiber volume fraction is the fraction of the mold volume occupied by the preform. This is one of the many parameters affecting the pressure distribution in the mold.

1.3 Background

1.3.1 Permeability measurements

For layered preforms, permeability measurements can be broadly classified into:

(i) in-plane permeability measurements and

(ii) transverse permeability measurements.

In the former, the principal direction of flow is in the plane (x-y) of the layers; hence the name. A number of in-plane permeability studies have already been carried out [2-6] and a variety of preforms have been used in these studies. Some researchers have correlated the in-plane permeability to the fiber volume fraction of the layers [5&7]. There is a general acceptance of the fact [7,30] that the classical Karman-Cozeny equation, given below, is a good model for predicting the planar permeability.

$$K_{ii} = \frac{r_f^2}{4k_{ii}} \frac{(1-V_f)^3}{V_f^2} \qquad (1.1)$$

Here K_{ii} is the in-plane permeability, r_f is the tow radius, V_f is the fiber volume fraction and k_{ii} is the so-called Kozeny constant. Different groups [7,10] use a different value of Kozeny constant to fit their planar permeability data. Gutowski et al. [7] have used a value of 0.7 whereas Skartsis et al. [30] mention that k_{ii} can have a value of 4-5.

However, the point remains that the in-plane permeability data can be fitted to the fiber volume fraction using equation (1.1).

In contrast, not enough data exists on transverse permeabilities. The existing data are described briefly in Table 1.1. A lot of data [4,8] reported on transverse permeability measurements are now known to be plagued by channeling. Channeling is a process in which the resin manages to find certain paths through and around the preform, of relatively less resistance. Most of the fluid follows these paths and the permeability observed is much higher than that would have been seen without channeling. Data free of channeling have been reported in [9,10].

Morse et al. [9] have used preforms consisting of a variety of fiber mats (0° & 90° stitched, weave and random). A fixed fiber volume fraction of 0.35 has been used. Transverse permeability measurements have been made and an empirical relation has been proposed relating the permeability of the stack to the fiber volume fraction of each layer used.

Trevino et al. [10] have used unidirectional, bidirectional and random glass fibers (fiber volume fraction 0.2 to 0.45) and have carried out permeability measurements on each of these. The effect of stacking sequence on the permeability is the main consideration here. A relation to determine thickness of each individual layer during flow experiment, has been developed. This has been related to individual layer permeability and then to the stack permeability.

Kim et al. [17] have also used various types of fiber mats and have studied their transverse and planar permeabilities. Expressions for determining the average stack

permeability using individual layer thicknesses and permeabilities have been developed. A fiber volume fraction range of 0.3 to 0.4 has been used.

In contrast to the above studies, the present work employs the same type of layers to build up the preform, thus eliminating the need to develop expressions relating average permeability of stack to that of individual layers. A higher set of fiber volume fractions (0.4-0.6) has been used, since no data are available for this range. The effect of varying fiber volume fraction of the preform on transverse permeability has been studied and quantified here. This is particularly essential because the Karman - Cozeny equation fails to predict the transverse permeability as a function of fiber volume fraction. In addition, special attention has been paid towards the elimination of channeling effects.

Table 1.1 Permeability measurements carried by other workers

Author	Ref. no.	Fiber	Resin	V_f	In-plane	Trans.
Kim	17	B[1], GR[2]	Corn oil	0.3-0.4	Yes	Yes
Trevino	10	GR, S[3]	DOP oil	0.2-0.45	Yes	Yes
Molnar	4	B,GR	DOP oil	0.1-0.2	No	Yes
Skartsis	8	C[4]	Silicone oil	0.5-0.7	Yes	Yes
Lam	13	C	Silicone oil & water	0.5-0.7	Yes	Yes
Morse	9	GR,B,S	Turbine oil	0.35	No	Yes

1:Bidirectional 2:Random glass 3:Stitched 4:Aligned Carbon

1.3.2 Preform compaction and channeling

Compaction may be stated as the phenomenon wherein the preform is compressed in the mold, during flow operation. This results in an increase in the fiber volume fraction of the preform, leading to a decrease in the permeability.

The process can be better explained by considering Darcy's law again:

$$Q = K_{zz}\frac{A_f}{\mu}\left(-\frac{\Delta P}{t_f}\right) \tag{1.2}$$

Here Q is the flow rate of the resin, A_f is the cross-sectional area of the preform, μ is the viscosity of the resin, ΔP is the pressure drop across the thickness t_f of the preform. For a given thickness, viscosity and cross-sectional area, the pressure drop should be a linear function of the bulk velocity (Q/A_f), with a slope given by ($K_{zz}/\mu\ t_f$). At low flow rates, this is observed to be true. However, at higher flow rates, a deviation from the straight line behavior has been observed [9,10]. This is shown schematically in Figure 1.1a. In case channeling of the fluid does occur, a trend opposite to the one shown is observed [4] (Figure 1.1b). This is because channeling leads to a greater flow rate at the same pressure drop, thereby causing an increase in the apparent permeability, which is shown as an upward deviation on a pressure drop - flow rate plot.

During compaction of the preform, a part of the applied pressure is carried by the fibers. This is called the effective stress. A detailed study of this has been done by Gutowski et al. [7,19]. Here, pressure is applied on the preform by mechanical means. It has been shown that the effective stress carried by the fibers increases with V_f.

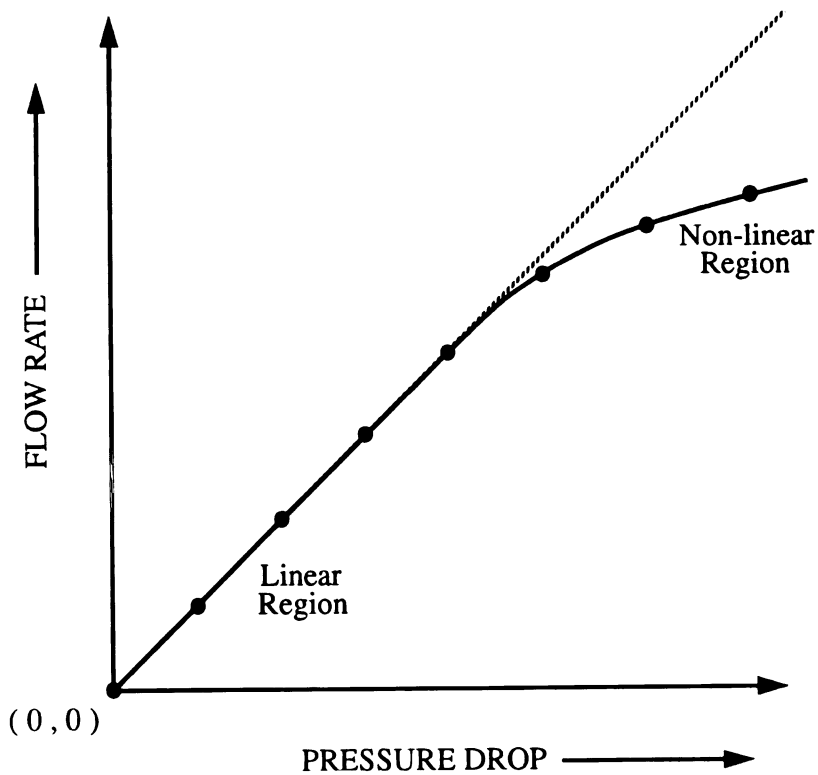

Figure 1.2a Typical flow curve (Schematic)

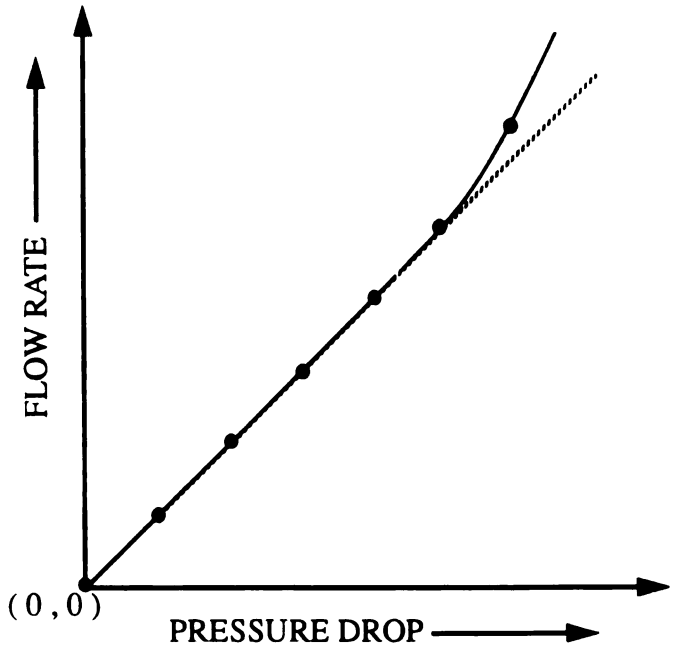

Figure 1.1b Channeling effect (Schematic)

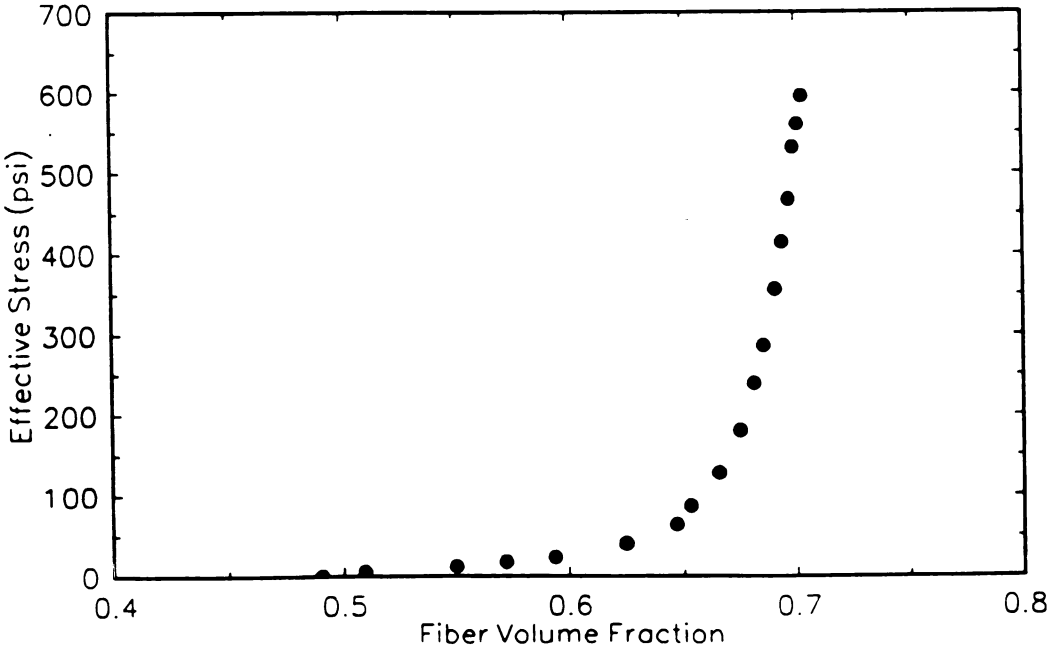

Figure 1.2 Typical compaction data [7]

However, after a certain fiber volume fraction is reached (denoted by V_a), an infinite stress is carried by the fibers. This is shown in Figure 1.2. A model has also been proposed relating the effective stress carried by the fibers to the fiber volume fraction. The details of this model are discussed in Chapter 4.

Trevino et al. [10] and Skartsis et al. [8] have also carried out compaction studies on continuous, random fiber mat layers. The source of compaction used in their studies is a mechanical tensile/compression tester. The similarity of all these three experiments [7,8,10] is that there is no continuous flow of resin through the preform. Compaction takes place only due to the mechanical load used. Thus, there have been no results presented so far linking the preform compaction to actual flow conditions. The present work quantifies the compaction effects resulting from resin flow through the thickness of the preform.

Many workers [5,9] have neglected the change in thickness of the preform during compaction, while computing permeability. Although this approach simplifies the calculations, it leads to incorrect results. The present study has incorporated varying thickness into permeability computations.

1.4 Objectives

The objectives of the present study are :

(1) To obtain transverse permeability data for stacks of continuous strand fiber mats over a range of fiber volume fractions (0.4 to 0.6).

(2) To develop a model predicting the experimental permeability as a function of the process variables.

(3) To study the effects of varying initial fiber volume fraction and resin viscosity on the compaction of these stacks.

(4) To explore the consequence of preforming history on the permeability and compaction.

(5) To develop a model relating effective stress carried by the fibers to fiber volume fraction, for compaction along the flow direction, during permeation experiments.

(6) To predict the entire pressure drop - flow rate curve as a function of preform and resin properties.

Chapter 2 Experimental Arrangement

The experimental configuration and materials used for the determination of transverse permeability are described in this chapter.

2.1 Materials

Continuous strands of random glass fibers, provided by Vetrotex Certainteed (U-101), were used as the preform mats. These mats have high solubility in styrene and have a surface density of 0.405 kg/m^2. The mats were available as 50" wide rolls. Small pieces, matching the requirements of the experiment, were cut off from this roll.

A mixture of glycerol and water was used to simulate the viscosity of the resins employed in SRIM processes. Viscosity of this solution was varied by changing the water content. For most of the runs, a constant viscosity of 75 mPa-s (as measured by a Brookfield viscometer) was used. A few runs also used solutions of viscosities 180 and 360 mPa-s. Glycerol - water mixture was found to have a constant viscosity in the shear rate range of 0.1 - 30 s^{-1}. Density of the solution varied between 1.05 to 1.2 gm/cm^3, depending on the concentration.

To provide effective sealing, Dow Corning's Silicone sealant and vacuum grease were used. These are necessary to prevent channeling effects.

2.2 Experimental setup and procedure

2.2.1 Experimental flow-loop

Figure 2.1 shows the experimental flow-loop schematically. The fluid is transferred from a container to a stainless steel reservoir (volume 85 lit) by a pump. It then flows through a cell designed to hold the preform and is subsequently recycled to the drum. Flow takes place in the direction of the thickness of the preform. No gravity effects are involved. Care is taken to prevent any glycerol loss in the process by running the entire system in a closed loop. The fluid is forced into the permeation cell in one of two ways. A constant volume - displacement pump (Moyno pump) is used for lower flow rates (up to 7 cm^3/s). For higher flow rates, compressed Nitrogen is used to force the liquid. A regulator is used to maintain constant pressure on the liquid. The desired pressure in the reservoir can be easily changed by help of a valve attached to the regulator. Special tubing (Tygon R-3603 / Kuritec K3150) is employed to withstand the high pressures.

2.2.2 Preform assembly

Figure 2.2 shows the half cross-section of the preform assembly. This assembly consists of two rectangular plates (Aluminum, 15x9x1.27 cm^3), each having grooves as shown in the figure. A central hole is bored in both the plates. Two porous plates, (Aluminum, 7.6x6.6 cm^2) having 24 circular holes (diameter 0.635 cm) each, are placed in the grooves and are tightened to the outer plates by means of screws. This leaves a small cavity (2.4 mm deep) between the two porous plates. The porous plates have two

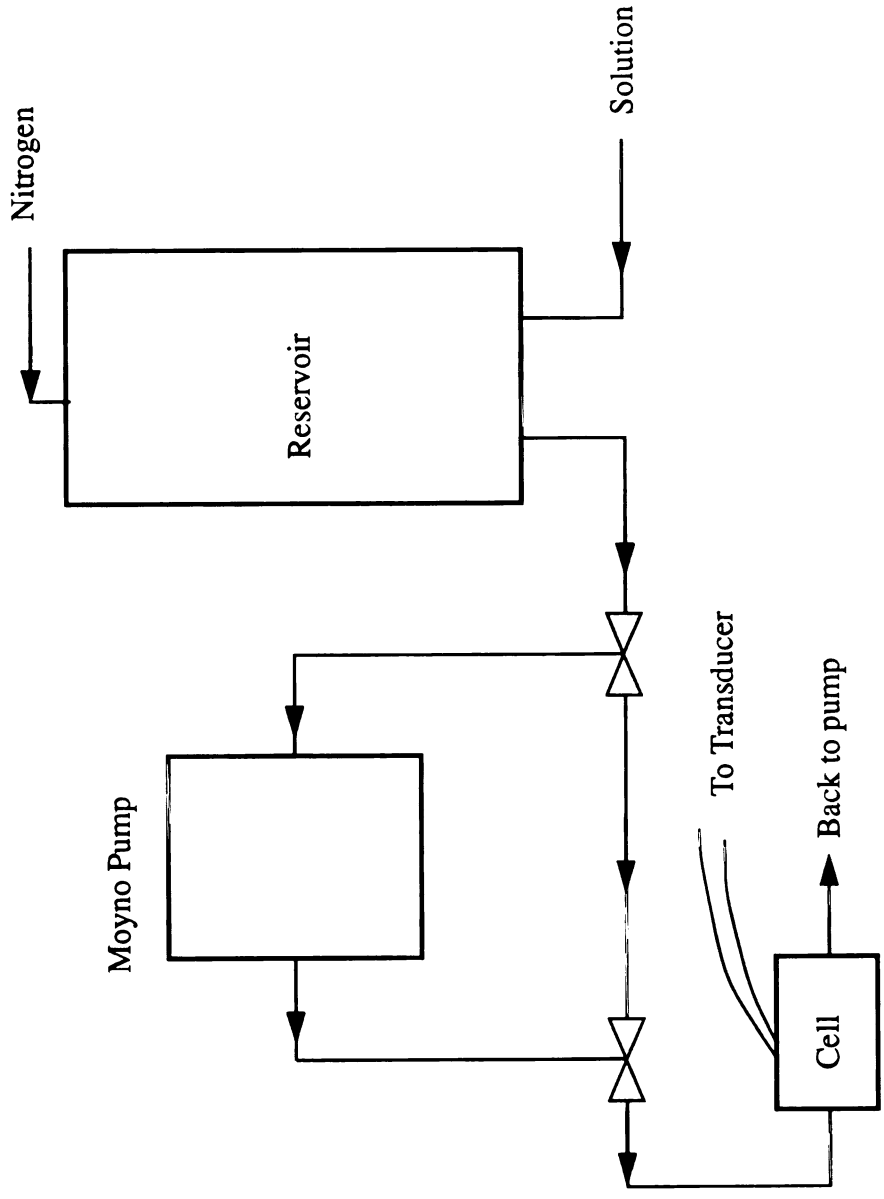

Figure 2.1 Schematic of flow loop

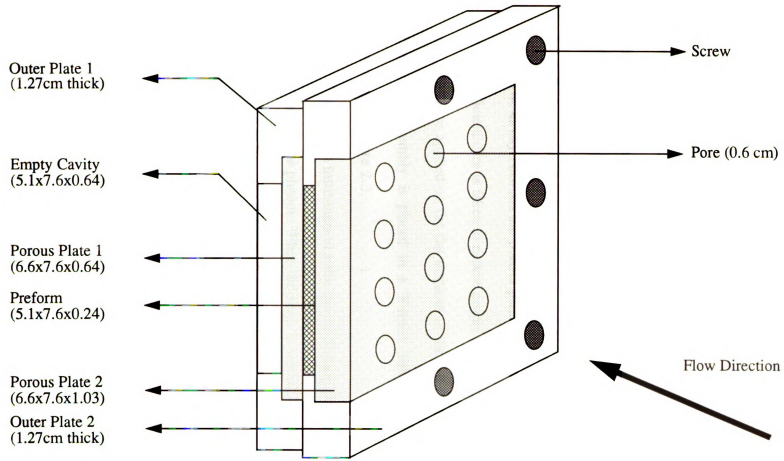

Figure 2.2 Preform assembly (Half Section)

functions : (i) to uniformly distribute the fluid throughout the preform surface (ii) to maintain the thickness of the preform. Since the preform is to be held between the two porous plates, sufficiently thick (0.635 cm) porous plates are selected to ensure the second function mentioned above. The additional pressure drop caused by the porous plates was calculated and the maximum value obtained was less than 3% of the applied pressure drop. Hence, it can be safely neglected.

2.2.3 Preforming technique

The cavity between the porous plates is filled with the required number of fiber mats. Sufficient care is taken to ensure proper alignment of the two outer plates. Sealant and grease are applied on the flat surfaces of the two plates in contact with each other. The whole assembly is placed in a Wabash instrumented press. This assembly is illustrated in Figure 2.3.

The Wabash instrumented press has the feature of preselecting a set-point load and a closure rate of the platens. When the press is started, the lower platen moves upward and the object in between the platens is compressed. When the load set-point is reached, no further increase in loading takes place. The platens still continue to move towards each other at a slow, constant speed.

A wooden support placed on the top plate gives enough room for a screw driver to tighten the assembly. A loading force is applied on the outer plates, due to which the thickness of the preform stack is reduced. The load is increased gradually till the preform fits in the cavity provided for it. When the two plates touch each other, the entire

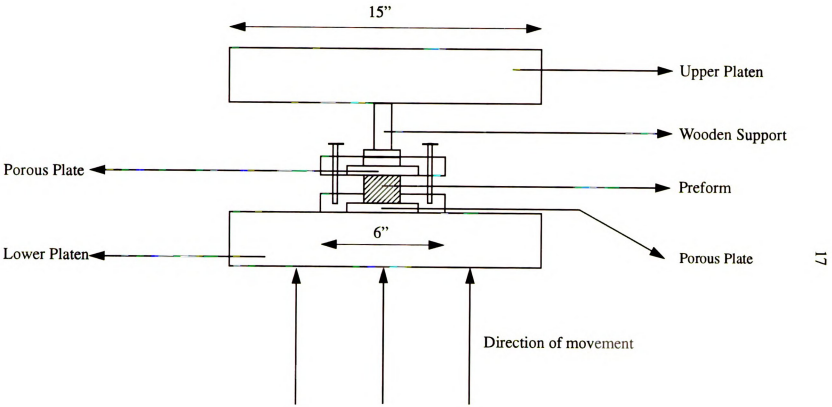

Figure 2.3 Preform preparation

assembly is tightened by means of screws. The load that has been applied is noted. This is called the preforming load. Since the volume of the preform is fixed (equal to the cavity volume), the preforming load depends on the number of layers of the mats used. For the present study, six to ten layers were used.

2.2.4 Final assembly

This tightened assembly fits into a slot in the rectangular box (cell) made of Aluminum plates (1.27 cm thick). The box has dimensions of 25.4x17.8x12.1 cm^3. Sealant is applied all around the contact points between the assembly and the cell walls. The whole setup is allowed to stay for 24 - 30 hours, since the curing time of the sealant is 24 hours. Two tapped holes on either side of the assembly accommodate the transducers used to measure the pressure drop across the preform. Sealant is also used around the transducer fittings to prevent any leakage of the fluid. Use of sealant at all metal - metal contact points is very important. This ensures that the fluid passes through the preform without finding any other path, thereby avoiding channeling.

2.2.5 Experimental measurements

Fluid is passed into the cell and kept for about 15 minutes to saturate the preform. The outlet valve is then opened. Steady state requires about 2 to 3 minutes to be achieved. Flow rate of the fluid is measured at the exit of the cell, by means of graduated cylinders. After the flow rate is increased, steady state is allowed to reach before any kind of measurement is made. Steady state conditions can be made out when the pressure

readings shown by the transducers stop changing. Thus, the raw data consists of flow rates measured at various pressure drops. In the present case, the flow rates used ranged from 4 to 135 cm^3/s. The corresponding pressure drops varied between 4 to 70 psi.

A critical requirement here is the prevention of channeling of fluid from the top, bottom and sides of the preform. To this effect, extra care was taken to obtain a very tight fit between all metal - to - metal contacts. Also, as mentioned earlier, sealant was used to seal all the possible gaps through which channeling could occur.

2.2.6 Fiber volume fraction calculations

The fiber volume fraction can be calculated by using the following relation -

$$V_f = \frac{m_f}{t_f A_f \rho_f} (1 - w_b) \qquad (2.1)$$

Here m_f is the total mass of the preform, t_f is the thickness of the preform (0.2375 cm), A_f is the cross-sectional area of the preform (36.21 cm^2) and ρ_f is the density of E-glass fibers, which is taken from literature [2] as 2.56 gm/cm^3. w_b is the weight fraction of the binder present in the preform. For the present case, w_b is 0.048. Except for m_f, all other quantities are constant. Therefore, to vary the fiber volume fraction the only parameter that can be changed is m_f. This is done by changing the number of fiber mat layers used. Thus, a whole range of volume fractions can be achieved. In the present case this ranges from 0.4 to 0.6. The advantage of using a high V_f range is that the flow rates that have to be dealt with are low and are therefore easy to measure.

Once a preform has been prepared, all the parameters in equation (2.1) become constant. If the fiber volume fraction of this preform is to change for some reasons, it can only do so through the thickness, t_f. Hence, equation (2.1) can be written as -

$$V_f = \frac{c}{t_f} \tag{2.2}$$

Here the constant c is given by -

$$c = \frac{m_f}{A_f \rho_f}(1 - w_b) \tag{2.3}$$

Relation (2.2) will be used extensively in future sections.

2.3 An earlier preform assembly design

The assembly described above, did not come about in the first attempt. An earlier version used to generate data is described below.

Instead of the preform being placed in a cavity, it was kept in between the two porous plates and the entire assembly was tightened as before. Thus, if one of the outer plates shown in Figure 2.2 were to be rotated by 180°, the earlier assembly would be obtained. In this older version, there was no restriction on the thickness of the preform. Eight layers of mats were used to make up the preform. Changing the thickness of the preform resulted in various fiber volume fractions. Using this setup, a V_f range of 0.2 - 0.6 was used. Flow rates varied from 4 to 250 cm^3/s with corresponding pressure drops from 3 to 127 KPa.

The shortcomings of this type of assembly were :

(i) Since the preform area was larger than the cavity area, the flow that took place was not purely transverse. Part of the liquid did flow in the x-y plane before exiting from the other side. It has been shown [10] that the planar permeability is higher than transverse permeability. This, therefore, resulted in an apparent transverse permeability that was higher than the actual transverse permeability.

(ii) Instead of a metal - to - metal contact between the assembly and the permeation cell walls, now there was an additional fiber - to - metal contact. There is no effective means of sealing such a contact junction. As a result, channeling did take place and again the result of this was to increase the "transverse" permeability.

The combined effect of these shortcomings was to drastically increase the transverse permeability. A new design had to be arrived at, to take care of both points mentioned above. The new design (described in section 2.2) rectified both these disadvantages effectively. Since the preform was enclosed in a cavity, there was no fiber - metal contact. Also, equality of dimensions of porous plates and preform ensured that all the fluid had to pass only through the thickness of preform. All the data reported in the present work have been obtained using the modified preform assembly. The permeabilities obtained by both arrangements are compared in Figure 2.4. Permeabilities upto 4 - 8 times larger were obtained using the older design. The method for calculation of permeability has been demonstrated in section 3.1.

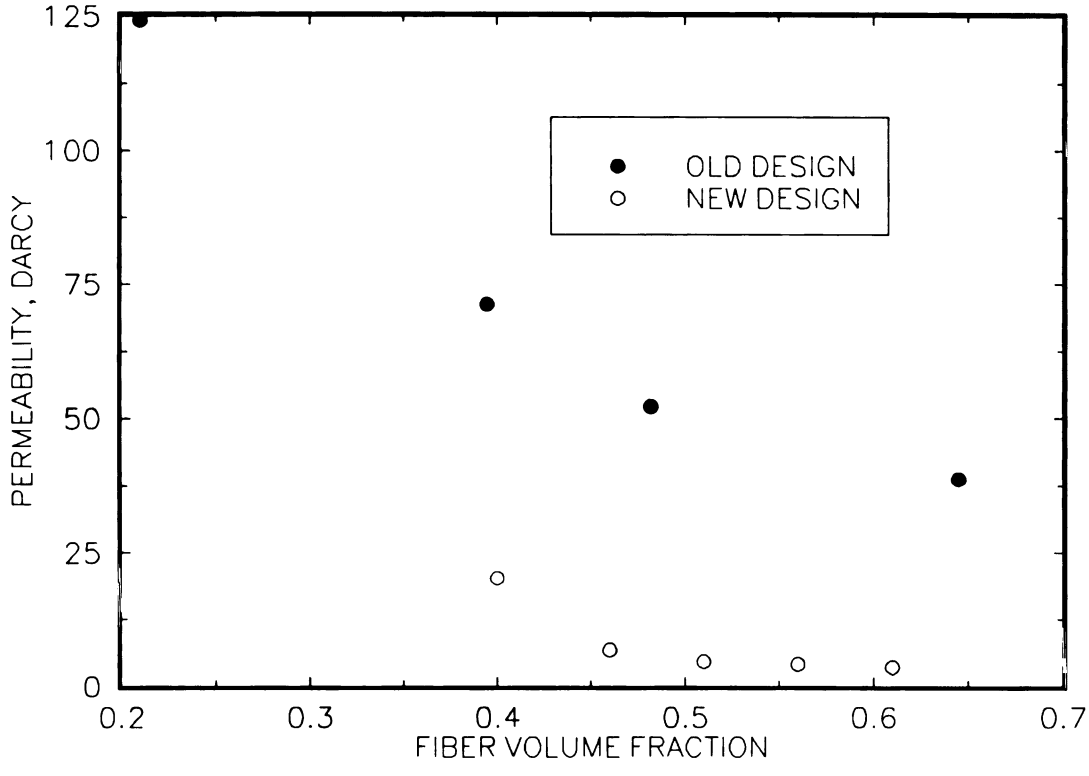

Figure 2.4 Effect of cell design on permeability

2.4 Fluid-fiber interaction

Another important consideration is the interacting force between the fibers and resin used. To compare the degree of interaction, wicking experiments were carried out using the glycerol-water solution, corn oil and Derakane 411-C50, a commercial resin currently used in many liquid molding processes. The method used here has been suggested by Chwastiak [14]. Details of the experiments are shown in the Appendix 1.

Table 2.1 gives the equilibrium contact angles (θ) obtained for all the three fluids used. Surface tension for glycerol-water solution has been calculated using empirical relations from [29]. [23] gives surface tension values for oils. The value for Derakane has been taken from the unpublished work of Brent Larson.

$\Delta\gamma_{avg}$ is the difference in surface free energy between a unit area of dry surface and a unit area of wetted surface. This is the parameter that follows from the experiment described in Appendix 1. The equilibrium contact angle is then obtained by :

$$Cos\theta = \frac{\Delta\gamma_{avg}}{\gamma_l}$$

Here γ_l is the surface tension of the liquid used.

A higher equilibrium contact angle (closer to 90°) implies poor wetting. Table 2.1 indicates that best wetting results are obtained for corn oil. However, glycerol-water solution, though with the least wetting capabilities, has a contact angle close to that of Derakane. Thus, if permeation is affected by fiber-fluid interaction, one can say that this effect will not have a significant role in differences between permeabilities obtained using

glycerol-water solution and Derakane as the fluids.

Table 2.1 Results of wicking experiments

Liquid	Surface tension (dyne/cm)	$\Delta\gamma_{avg}$ (dyne/cm)	θ (°)
Derakane	32	10.17	63.3
Glycerol-Water	66	30.12	71.5
Corn oil	21	15.15	43.8

Chapter 3 Permeability Data and Prediction

This section describes the calculation of the transverse permeability, compares the results with those obtained by other workers and finally proposes a model for the permeability as a function of fiber volume fraction.

3.1 Data obtained and permeability calculations

Pressure drop - flow rate data obtained for a fiber volume fraction range of 0.4 - 0.6 are shown in Figure 3.1. For each value of fiber volume fraction, the entire plot can be divided into two parts : (i) a linear region passing through the origin and (ii) a nonlinear region exhibiting the compaction effects mentioned previously. The nature of the curve observed at higher flow rates, corresponds to the case without channeling.

Transverse permeability can be calculated using the slope of the linear portion of the curve and Darcy's law. Equation (3.1) represents the rearranged form of Darcy's law, which is used for this purpose. Information provided by the nonlinear region is discussed in chapter 4.

$$K_{zz} = \left[\frac{Q}{(-\Delta P)}\right] \frac{\mu}{A_f} t_f \qquad (3.1)$$

μ, A_f and t_f are known constants. The slope of the linear portion obtained from Figure 3.1 may be substituted in the above equation to yield the permeability. The SI unit

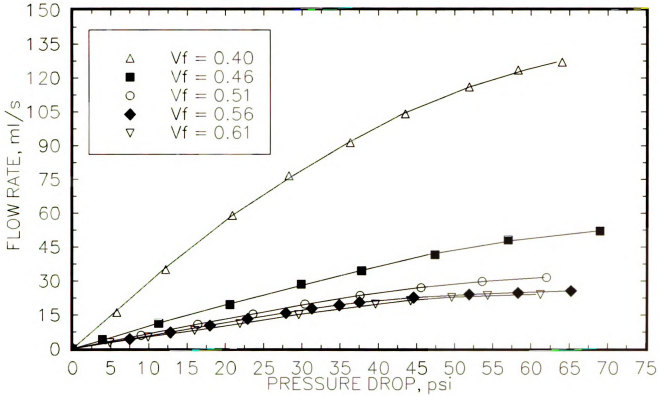

Figure 3.1 Flow rate - Pressure drop data

of K_{zz} is m^2. However, permeability is very commonly reported in units of 'Darcy'. A Darcy is the permeability which would allow a linear velocity of 1 cm/s under a pressure gradient of 1 atm/cm for a fluid of viscosity 1 mPa-s.

$$1\ Darcy = 1\frac{cm}{s}\ \frac{1 mPa\text{-}s}{1\frac{atm}{cm}}$$
$$= 9.87\ x\ 10^{-13}\ m^2$$

Due to the significant difference seen in the curves (Figure 3.1) of fiber volume fractions 0.40 and 0.46, a precision of four decimal places for describing the volume fractions, was selected for all calculations. Since different fiber volume fractions have different flow rate - pressure drop profiles, it follows that the permeabilities vary with volume fractions. A plot of the permeability calculated as a function of the varying fiber volume fraction is shown in Figure 3.2. As V_f is increased, the permeability drops down. This makes sense because higher volume fractions mean lesser available volume for the fluid to pass through, i.e., lower permeability. At the higher end of V_f (close to 0.55 - 0.6), the fall in the K_{zz} value is not as drastic as compared to the fall between 0.4 - 0.5. This is explained later in section 3.2.

Table 3.1 lists the transverse permeability obtained by other workers. It is observed that permeability is fairly high at very low fiber volume fractions. It should be pointed out that almost none of the fibers used by the listed workers, are of the same commercial brand. Hence, same values of permeability cannot be expected. Morse et al. [9] and Kim et al. [17] report data closest to that obtained in the present study.

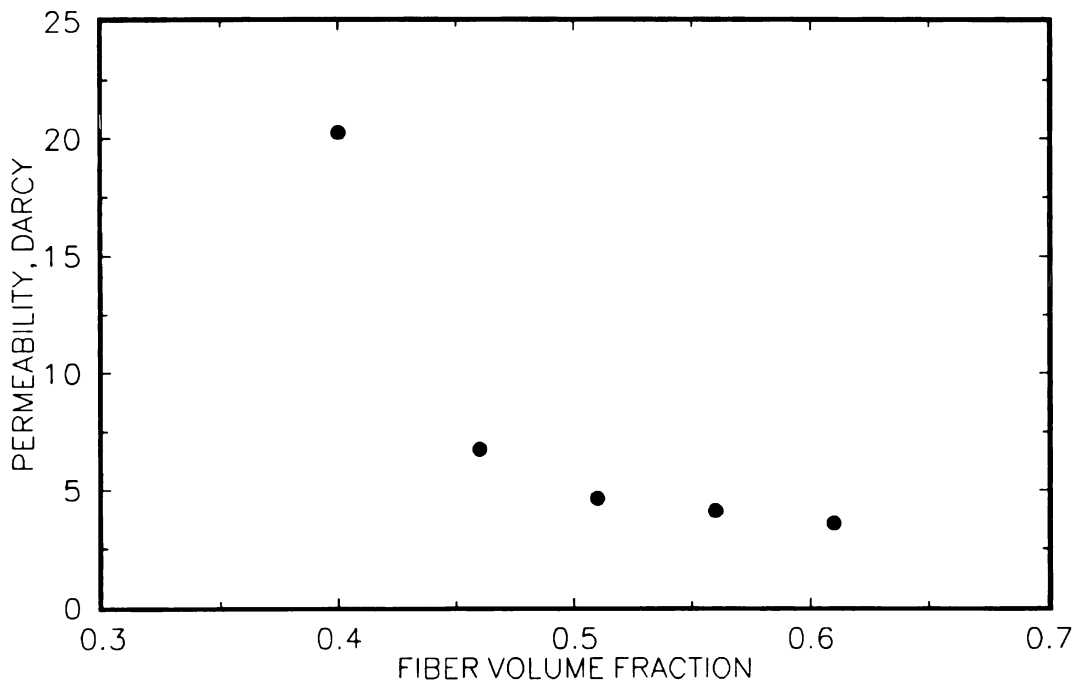

Figure 3.2 Permeability calculated from data

The permeability results obtained with the older assembly design have been shown in Appendix 2.

Table 3.1 Transverse permeability comparison

Reference	V_f range	K_{zz} range(Darcy)	Type of fiber
Trevino[10]	0.2 - 0.5	1000 - 3000	Glass - Random
Molnar[4]	0.1 - 0.2	500 - 1000	Glass - Random
Skartsis[8]	0.5 - 0.7	0.1 - 0.3	Carbon - Aligned
Lam[13]	0.5 - 0.7	0.1 - 10	Carbon - Aligned
Morse[9]	0.35	6 - 20	Glass
Kim[17]	0.3 - 0.45	5 - 20	Glass - Random
Present	0.4 - 0.6	4 - 20	Glass - Random

3.2 Modeling of permeability

The classical Karman Cozeny equation (equation 1.1) was used as a starting relation between the permeability and the fiber volume fraction. This equation is applicable for any porous media.

$$K_{zz} = \frac{r_f^2}{4k} \frac{(1-V_f)^3}{V_f^2} \qquad (1.1)$$

The best possible fit using this equation is shown in Figure 3.3a. Although this equation provides good results for flow taking place along the fiber length, its inability

to accurately predict the transverse permeability has already been reported by other workers [5,7]. This equation is based on the assumption that the preform can be equated to a system of parallel capillaries, the diameter of which is related to the hydraulic radius of the system. Hence, this representation is not really suitable for a bed of randomly arranged fibers. This explains its inability to act as a model for permeability prediction in the present case.

A bed of perfectly aligned fibers has a certain maximum possible packing, beyond which the fiber volume fraction cannot be increased [5]. Even in this condition, channels of capillaries in the fiber direction are present. Theoretically, flow in the direction of the fibers, therefore, cannot have a zero permeability even at the maximum packing fraction. A perfectly hexagonal packing has a maximum fiber volume fraction of 0.9069 [15]. Fibers arranged in a square array, have a maximum packing of 0.785 [15]. The maximum possible volume fraction for random fibers is believed to lie between these two limits [15]. In the case of flow transverse to the fiber length, however, the permeability may reach a zero value at the maximum packing fraction (less than one). Berdichevsky and Cai [11] have shown that if permeability is plotted as a function of fiber volume fraction on a semi-log plot, then the difference in the longitudinal and transverse permeability behavior is clearly brought forth. Whereas in transverse permeation, the permeability falls down to zero at higher volume fractions, in planar permeation, the permeability never reaches zero. Any attempt to predict the transverse permeability should, therefore, incorporate this feature. As mentioned earlier, the Karman - Cozeny

equation predicts a zero permeability at a fiber volume fraction of one and hence doesn't portray a true picture.

As a next attempt, a modification of the Karman-Cozeny equation was tried. This has been proposed by Gutowski et al. [7].

$$K_{zz} = \frac{r_f^2}{4k_{zz}} \frac{(\sqrt{\frac{V_m}{V_f}} - 1)^3}{(\frac{V_m}{V_f} + 1)} \tag{3.2}$$

The fit obtained is shown in Figure 3.3a. This equation, too, fails to model the present permeability.

Kim et al.[17] proposed an empirical equation

$$K_{zz} = A(BV_m - V_f)^4 \tag{3.3}$$

to explain the permeability variation with V_f. Here A is a fitting constant and B, the fiber orientation constant, is such that $1 \leq B \leq 1/V_m$. For transverse flows, B is close to 1. For flow in the longitudinal direction, B approaches a value of $1/V_m$. Figure 3.3a shows the fit obtained using equation (3.3).

Figure 3.3a clearly shows that the Karman-Cozeny equation and its modifications fail to predict the transverse permeability of continuous glass fiber mats. Berdichevsky & Cai [11,16] have obtained equations for unidirectional arrays of rods. The theoretical expression proposed by Berdichevsky and Cai [16] is given by :

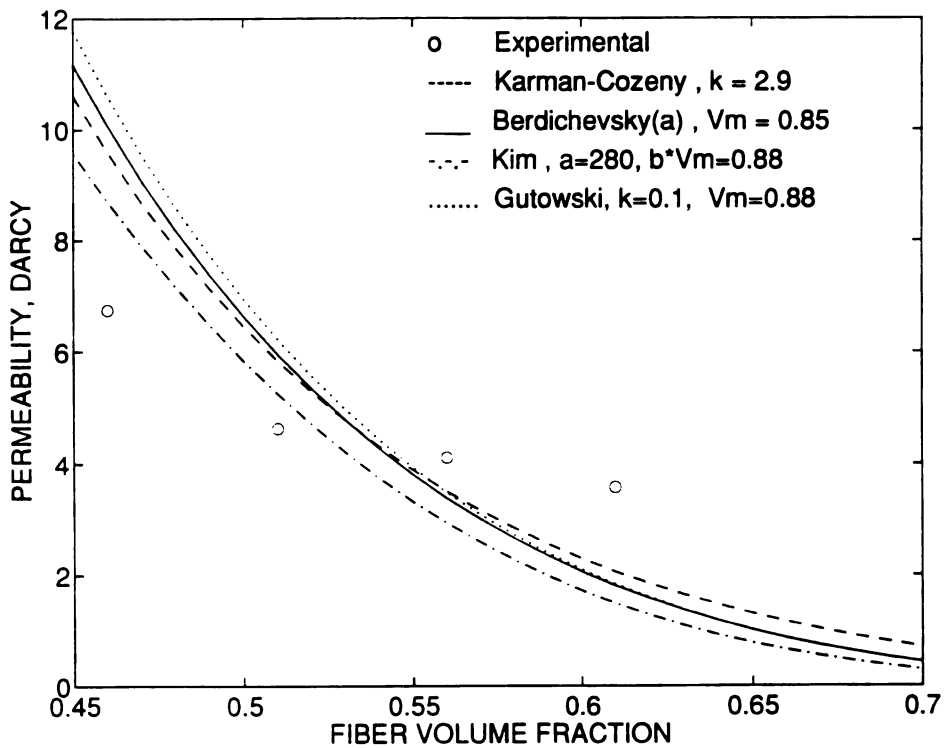

Figure 3.3a Permeability fitted with existing correlations

$$K_{zz} = 0.231\ r_f^2\ (-\ln\alpha)\ (1-\alpha)^{1.5}\ \left(\frac{2V_{ah}-V_m}{V_f}\right) \qquad (3.4\ a)$$

$$\alpha = \sqrt{\frac{V_f}{V_m}}$$

This model considers an insertion of a cylindrical micro-volume in a porous medium with homogeneous properties. This micro-volume represents the micro-structure of the porous medium. V_m is the maximum possible fiber volume fraction and V_{ah} is the maximum possible fiber volume fraction for a preform consisting of hexagonal arrays. r_f is the tow radius. Figure 3.3a shows the predicted permeability using equation (3.4a) and a value of 0.85 for V_m.

Another equation proposed by Berdichevsky & Cai [11] is based on finite element simulation of regular arrays of rods (square and hexagonal pitch). The authors have developed a relation for transverse permeability which is given below:

$$K_{zz} = r_f^2 A(V_m)\ \frac{\left(1-\sqrt{\frac{V_f}{V_m}}\right)^{\frac{5}{2}}}{\left(\sqrt{\frac{V_f}{V_m}}\right)^{n(V_m)}} \qquad (3.4b)$$

$$A(V_m) = 0.244 + 2(0.907 - V_m)^{1.229}$$
$$n(V_m) = 2.051 + 0.381\,V_m^{4.472}$$

Results using above equation, are shown in Figure 3.3b. A semi-log plot has been shown to compare the permeability trend with that shown in [11]. This equation, too, fails to predict the permeability for the range of fiber volume fraction used.

It is observed that none of these relations provide a satisfactory fit over the entire range of fiber volume fractions used. Changing the fitting parameters may bring about a better prediction for a particular range (lower or higher) of volume fraction, at the expense of accuracy in the other range. Therefore, none of the models can really be used to accurately predict permeability as a function of fiber volume fraction.

To predict the permeability effectively, an empirical model was developed. This three-parameter relation is given below :

$$K_{zz} = a(1 - \sqrt{\frac{V_f}{V_m}})^n \qquad (3.5)$$

Figure 3.4 shows the fit obtained by equation (3.5), using a value of 0.89 for V_m, 1.5 for n and 44 Darcy for a. Since the error involved in the permeability prediction is the least when equation (3.5) is used, this is the model of choice for future calculations. Note also that this equation predicts a maximum packing fraction of 0.89 which, although on the higher side, still lies between the values of square and hexagonal array packing.

In fitting equations (3.2 - 3.5) and (1.1), Marquardt's method for nonlinear regression has been used. This is invoked by the nonlinear regression analysis mode of the program PlotIT. A FORTRAN program was written to import the output of PlotIT and check for the set of coefficients yielding the minimum possible sum of squares of the errors. The best coefficients were returned by the program as its output. MatLab was

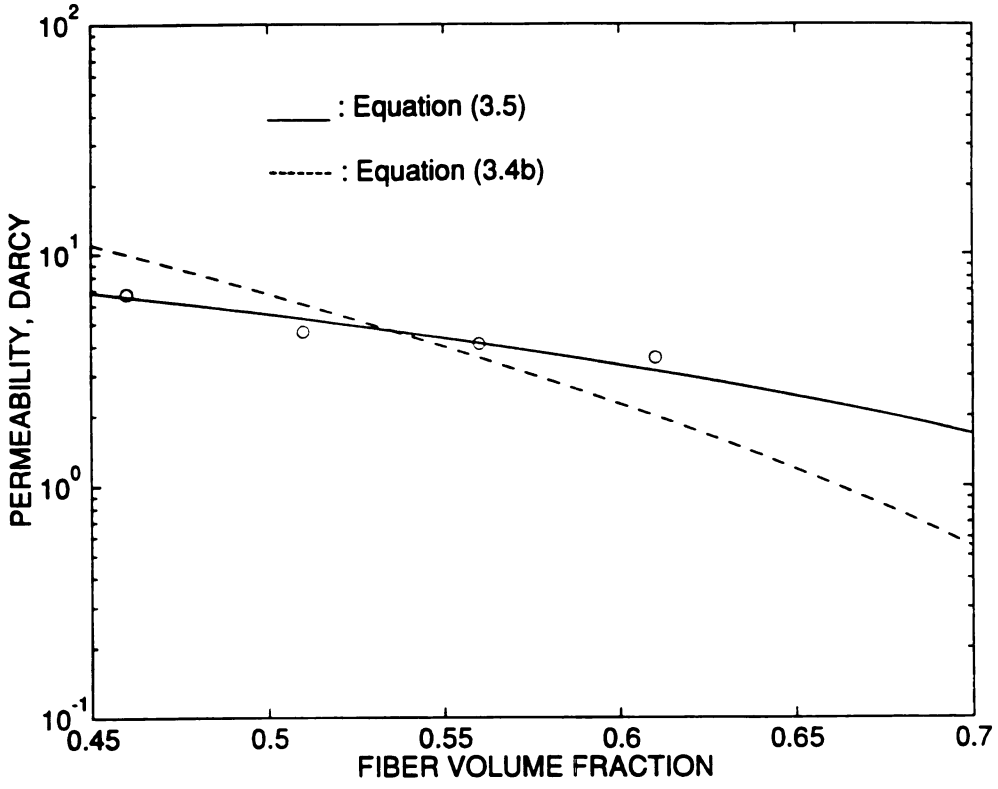

Figure 3.3b Permeability fitted with Berdichevsky's [11] equation

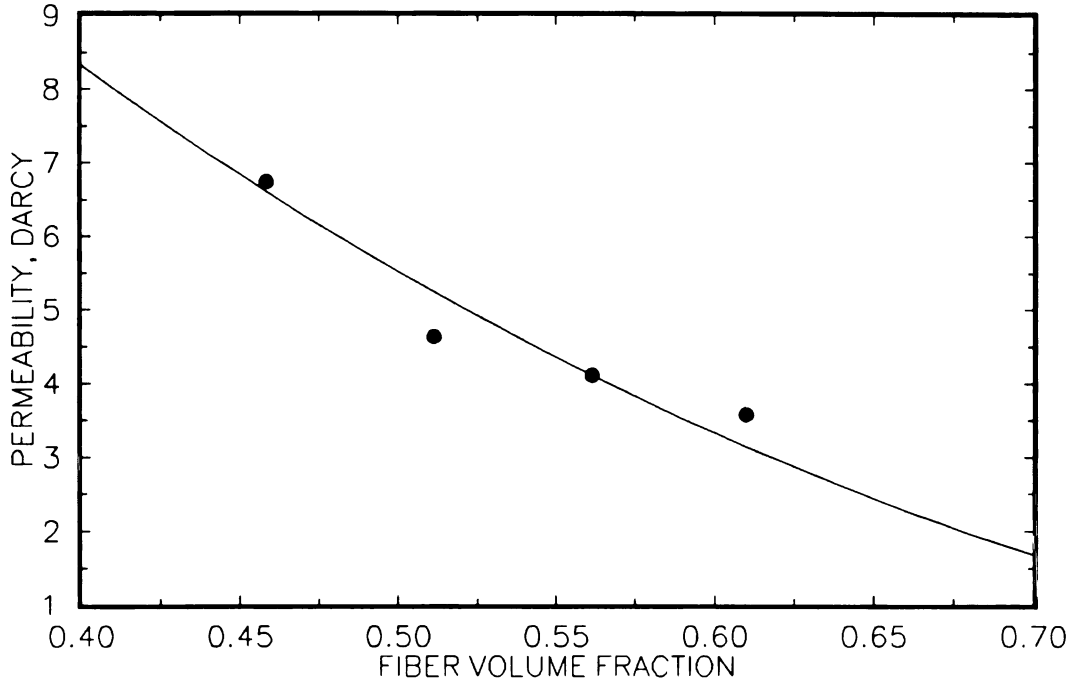

Figure 3.4 Fit obtained by equation (3.5)

then invoked to calculate the permeabilities using the available coefficients. Table 3.2 lists the various coefficients used to plot the curves shown in Figures 3.3a, 3.3b and 3.4.

As mentioned earlier, the nonlinear region of the pressure drop - flow rate curve is discussed in Chapter 4. Equation (3.5) is used, henceforth, to model the compaction effects.

Table 3.2 Fitting constants used in modeling permeability

Equation #	Constants		
1.1	$k_{zz} = 2.9$	-	-
3.2	$k_{zz} = 0.1$	$V_m = 0.88$	-
3.3	$A = 280$	$B*V_m = 0.88$	-
3.4a	$V_m = 0.85$	-	-
3.4b	$V_m = 0.86$	-	-
3.5	$a = 44$	$V_m = 0.89$	$n = 1.5$

Chapter 4 Compaction Effects

The phenomena of preform compaction at higher flow rates, effect of fluid viscosity on compaction, effect of hysteresis on the fiber volume fraction, modeling of the nonlinear region and prediction of the entire pressure drop - flow rate curve have been discussed in this chapter.

4.1 Previous Consolidation work

Gutowski et al. [7] have carried out consolidation experiments conducted on prepregs made of constant viscosity oils and aligned graphite fibers. In their set-up (Figure 4.1), the loose fiber mats are pressed by mechanical means. The resin pressure at the exit (P_r) is measured by a transducer. The thickness of the stack is related to the fiber volume fraction. Different applied loads result in different stack thicknesses and hence different fiber volume fractions. The difference between the applied load and the resin pressure is the stress carried by the fibers. Beyond a certain fiber volume fraction V_o, the effective stress is found to increase gradually with fiber volume fraction (refer Figure 1.2). At higher fiber volume fractions, there is a drastic increase in the ability of the fibers to carry the applied load. It has been shown that beyond a certain fiber volume fraction (V_s), no further increase in the fiber volume fraction takes place, even at very high applied loads. Thus, the maximum possible packing (V_a) comes into picture during

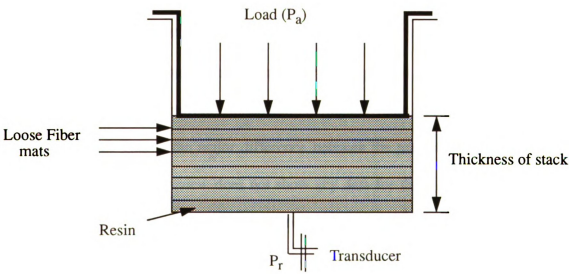

Figure 4.1 Schematic of Gutowski's [7] arrangement

compaction, too. Recall that a maximum packing (V_m) was used in equations relating the permeability to fiber volume fraction.

Kim et al. [17] have also carried out compression studies in a manner similar to that described above. They have used random, continuous glass mats with corn oil as the resin. They have observed a similar effective stress - fiber volume fraction behavior as in [7].

4.2 Compaction with through flow of resin

The present setup deals with preform compaction due to continuous flow of the resin through the preform thickness. A higher resin flow rate results in higher compaction. This is the major difference between the present work and that described above. A literature review does not show any data for this type of compaction. Figure 4.2a shows schematically the compaction effect on a pressure drop - flow rate curve. The nonlinear portion of the curve represents compaction of the preform. At lower pressure drops, the behavior can be represented by a straight line passing through the origin. However at some point, departure from linear behavior is exhibited. The pressure drop at this point is called the critical pressure drop and is denoted by ΔP_c. The corresponding flow rate is called the critical flow rate and is denoted by Q_c. Every initial fiber volume fraction (V_i) has a unique ΔP_c and Q_c associated with it. The actual flow curves exhibiting the compaction effects are shown in Figure 4.2b.

In the present setup, preforming is achieved by applying load on the stack in a Wabash instrumented press. This press has the feature of preselecting a set-point load and

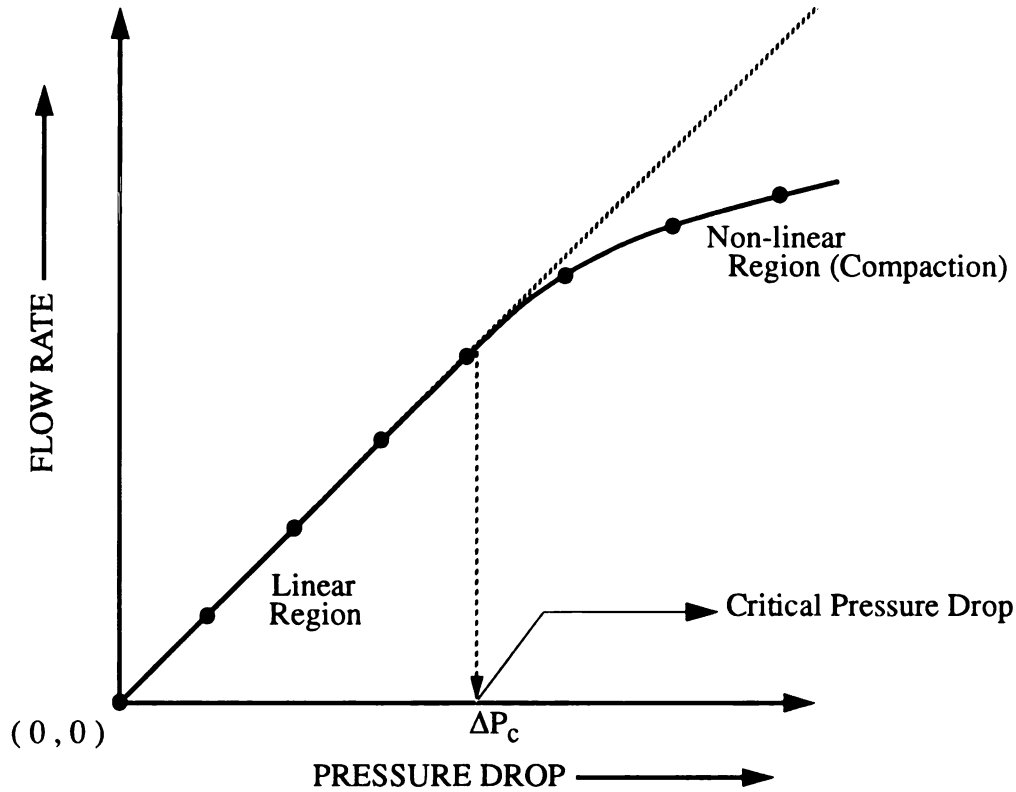

Figure 4.2a Typical flow curve (Schematic)

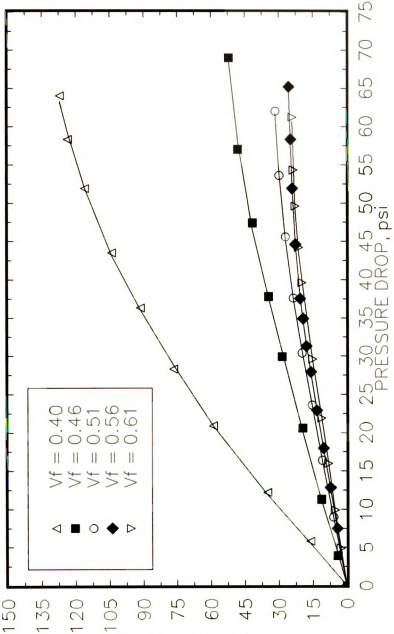

Figure 4.2b Flow curve showing compaction effect

a closure rate of the platens. When the press is started, the lower platen moves upward and the object in between the platens is compressed. When the load set-point is reached, no further increase in loading takes place. The platens still continue to move towards each other at a slow, constant speed. Preforming pressure is the preforming load divided by the platen surface area. The higher the fiber volume fraction needed, the greater is the number of fiber mats used to prepare the preform. This is so because the stack thickness is same in all the cases. Table 4.1 lists the critical pressure drop and the preforming pressure for various initial fiber volume fractions (V_i).

Table 4.1 Critical pressure drop & flow rate for various initial volume fractions.

V_i	ΔP_c (psi)	Q_c (ml/s)	Preforming Pressure (psi)
0.40	12.63	37.5	13.17
0.46	17.30	17.5	17.1
0.51	19.82	11.1	20.0
0.56	23.10	13.5	22.9
0.61	29.51	15.2	-

It can be seen that ΔP_c increases with the volume fraction. Further, when the critical pressure drop and the preforming pressure are plotted (Figure 4.3), a very interesting feature is seen. All the points lie close to the 45° line drawn through the

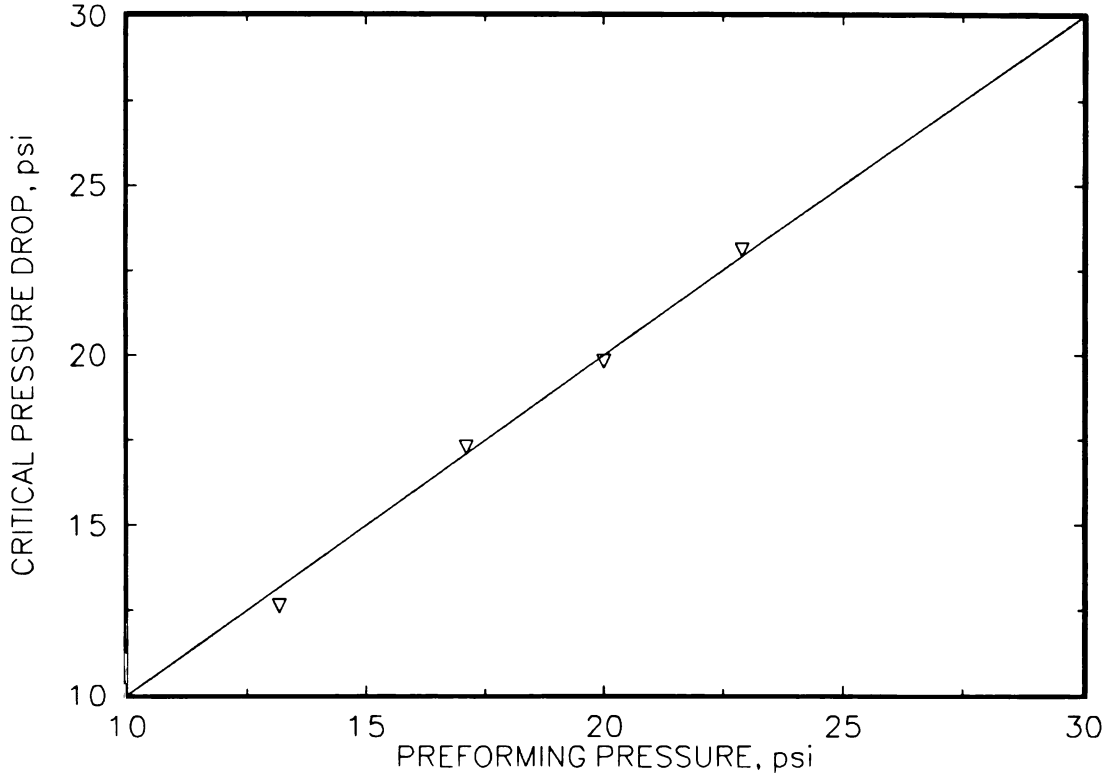

Figure 4.3 Equivalence of preforming pressure and critical pressure drop

origin. Thus, the closeness of both the parameters is clearly evident. They can be said to be equal parameters within the range of experimental errors.

This can only be explained if an analogy is drawn between mechanical loading (preforming) and the fluid pressure drop. In the former case, the load on the fiber stack is increased until the volume occupied by the preform is equal to that of the cavity (mold) between the two outer plates (Figure 2.2). Experimentally this can be determined by visual observation of the two outer plates in contact with each other. (After the loading operation, a micrometer screw gauge is used to check whether the two outer plates are really in contact with each other. This can be done because the total thickness of the preform assembly without any preform is already measured at twelve different locations. If the total assembly thickness with compacted preform is equal (at all twelve locations) to the previous values, then the two outer plates are in contact with each other throughout their surface). In this compacted position, screws are applied all along the periphery of the outer plates at ten locations. This holds the preform in position. Thus, there exists a definite load on the screws holding the preform in place. This load, theoretically equal to the preforming load applied, is called the initial effective load and when divided by the platen surface area is called the initial effective stress (σ_i). For fluid pressure drop less than this value, no load acts on the fibers because of the screws used. However, when pressure drop increases beyond the load borne by the screws (σ_i), the entire load (i.e., pressure drop) is transmitted to the fiber network, resulting in its compaction, or alternatively in an increase in fiber volume fraction, which leads to lower permeabilities, explaining the fall in the flow rate, beyond the critical pressure drop. This

explanation is proved by the equivalence of the critical pressure drop and the preforming pressure (Figure 4.3). Thus, for pressure drops less than the critical pressure drop, stress carried by the fibers is equal to the initial effective stress (or alternatively the critical pressure drop). For higher pressure drops, the entire pressure drop is the effective stress carried by the fibers.

Mathematically this may be stated as :

$$\sigma = \sigma_i = -\Delta P_c \ , \ for \ -\Delta P \leq -\Delta P_c$$
$$\sigma = -\Delta P \ , \ for \ -\Delta P > -\Delta P_c \qquad (4.1 \text{ a \& b})$$

Gutowski et al. [7] have shown that

$$P_a = P_r + \sigma \qquad (4.2)$$

Here, P_a is the applied pressure on the preform, P_r is the resin pressure at the exit and σ is the effective stress carried by the fibers. As mentioned in section 4.1, there is no clamping force on the preform structure (see Figure 4.1). Hence, there is no σ_i for the preform. The pressure drop (P_a - P_r), therefore, is equal to σ. It was further shown [7] that σ is zero below a certain fiber volume fraction (V_o). Thus, prior to the onset of compaction, the applied load doesn't result in any stress borne by the fibers. Once compaction begins, the pressure drop becomes equal to the effective stress on the fibers. Equation (4.2), thus, conforms to the present hypothesis suggested in equation (4.1).

Gutowski et al. [19] have modeled the effective stress - fiber volume fraction behavior, for their compaction experiments. The expression proposed is discussed in section 4.6 (equation 4.15). Since their preform compaction technique is similar to the preforming method followed in the present setup, it is expected that the σ_i and V_i values

should follow this relation. The fit obtained by using equation (4.15) is shown in Figure 4.3a. V_o (volume fraction at which loading begins) is the stack fiber volume fraction just before the platens start compressing the stack. This value is 0.05 for the present mats used. The fit uses V_a as 0.81 and β as 75, both of which are within the range obtained by Gutowski et al. in their studies.

Thus the important result that follows from this section is that the point at which compaction effects begin i.e., $(\Delta P_c, Q_c)$, can be predicted based just on the preforming load applied. The critical pressure drop is given by the preforming pressure from which the critical flow rate (Q_c) can be calculated by using Darcy's law.

4.3 Effective stress as a function of fiber volume fraction

At pressure drops lower than the critical pressure drop, the effective stress (σ) is equal to the initial effective stress (σ_i). At higher pressure drops, σ is equal to the pressure drop (equation 4.1 b). Darcy's law (equation 1.2) when substituted in equation 4.1 b yields

$$\sigma = -\Delta P = Q \frac{\mu}{A_f} \frac{t_f}{K_{zz}} \qquad (4.4)$$

μ and A_f are constants whereas K_{zz} and t_f vary with fiber volume fraction. These variations (equations 3.5 and 2.2) have been reproduced below -

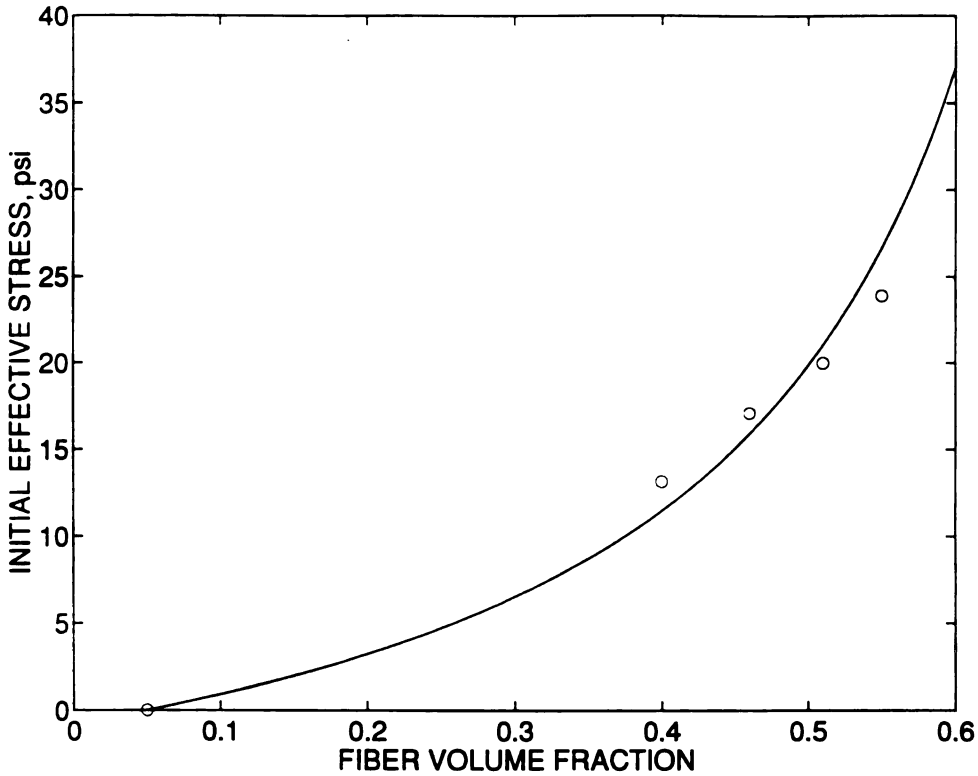

Figure 4.3a Compaction behavior during preforming

$$V_f = \frac{m_f}{\rho_f A_f t_f}(1 - w_b) = \frac{c}{t_f} \tag{2.2}$$

$$K_{zz} = a(1 - \sqrt{\frac{V_f}{V_m}})^n \tag{3.5}$$

Thus, for every curve shown in Figure 4.2b, equations (4.4), (3.5) and (2.2) may be solved to yield the fiber volume fraction at a given flow rate and pressure drop. A table of σ vs V_f may be generated from each curve. This was done with the help of the software MAPLE. The σ-V_f curves generated for a set of initial fiber volume fractions are shown in Figure 4.4. The trend observed is quite different from that obtained by Gutowski et al. [7] (Figure 1.2). The differences in experimental situations must be noted here. In the present set-up, applied pressure is due to the flow of the fluid across the preform. In [7], mechanical loading results in the applied load on the preform (refer Figure 4.3). Thus, the source of effective stress carried by the fibers is different in both cases. This might be responsible for the different trends in σ - V_f relationship.

Many workers [5,9] have neglected the change in thickness of the preform, while computing the permeability in the non-linear region. This is incorrect, since change in V_f can only be brought about by change in thickness, t_f (equation 2.2). This variation in thickness has to be incorporated in the permeability calculations, since change in permeability is exaggerated by not considering it. The present work, however, accounts for changing thickness, as shown above.

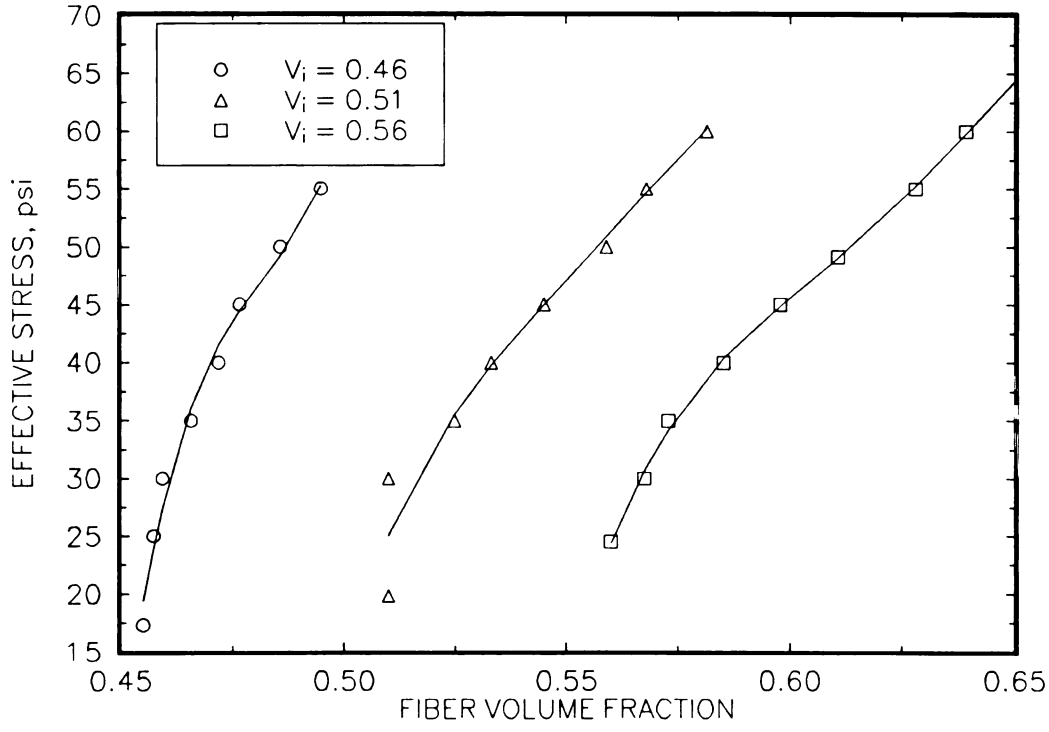

Figure 4.4 Calculated effective stress

4.4 Effect of fluid viscosity on compaction

To determine the effect of fluid viscosity on preform compaction, some runs with higher viscosity fluids were carried out. The same fluid was used but the concentration of glycerol was increased so that the viscosities of the resulting solutions were about 0.18 and 0.36 Pa-s. New preforms with same initial fiber volume fractions as before were made and pressure drop - flow rate runs were carried out in a similar manner as earlier. Figure 4.5 shows the data obtained. Darcy permeabilities in the linear region were found to be close to the values obtained with the lower viscosity fluid. However, compaction effects obtained were different. More compaction was obtained using the more viscous fluid, i.e., at the same pressure drop, the fiber volume fraction was higher for the case with more viscous fluid. This implies that in preforms where curing of the resin takes place, a lot of compaction might be taking place within the mold, thus affecting the geometry of the object. Hence, characterization of compaction (particularly with high viscosity fluids) assumes a significant role.

Another important point brought forth by Figure 4.5 is that the difference in compaction is much more at the lower end of initial fiber volume fractions ($\sim$40%). The curve with volume fraction of 0.51 is almost unaffected by fluid viscosity, even at higher pressure drops. Thus, working with a dense packing of fibers might be advantageous in countering the increase in fluid viscosity.

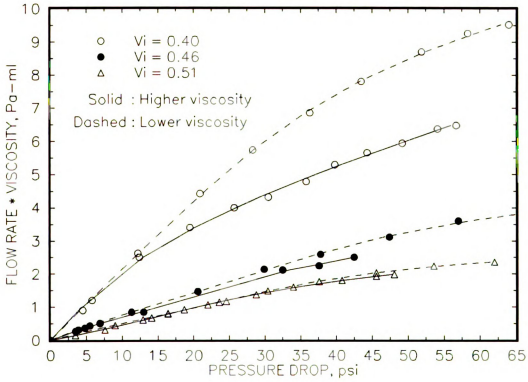

Figure 4.5 Effect of fluid viscosity on compaction

4.5 Hysteresis of flow

To obtain some insight into the nature of preforming history, a hysteresis test was performed on the preforms. Beginning at a minimum value, flow rate was increased slowly till a maximum possible value (limitation being the maximum pressure which the tubes could withstand). Pressure drop readings were simultaneously recorded. This is referred to as run 1. Flow rate was then gradually reduced to a minimum possible value and pressure drop readings were taken as before. This is run 2. This procedure was repeated till run 5. Data showing pressure drop vs flow rate is shown in Figures 4.6 a & b for two different initial fiber volume fractions. It is observed that a single run alters the structure of the preform, due to which subsequent runs result in different curves. Also, the departure from linearity takes place at a higher pressure drop in going from the first run to the fifth run. Runs 4 and 5 indicate an almost entirely linear behavior in the range of pressure drops studied. A straight line implies a constant permeability (or fiber volume fraction). Thus, every run results in compaction, causing a gradual decrease in permeability, with run 5 having a constant but lowest permeability. The preform seems to "remember" its recent volume fraction and even on decreasing the flow rate, never goes below the previous value.

The linear region was used to determine permeability for run 1. This was done using Darcy's law and the known initial preform thickness. For the second run onwards, equations (1.2), (2.2) and (3.5) were used to yield an equation with t_f as the only unknown. This was then solved to subsequently yield the values of the fiber volume fraction and permeability. Tables 4.2 and 4.3 show the various parameters obtained from

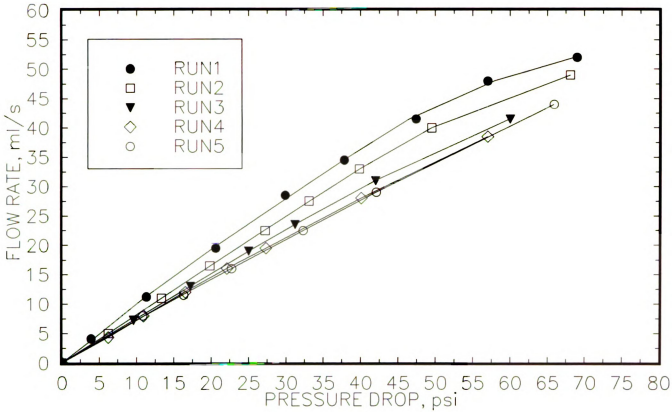

Figure 4.6a Hysteresis run (V_i = 0.46)

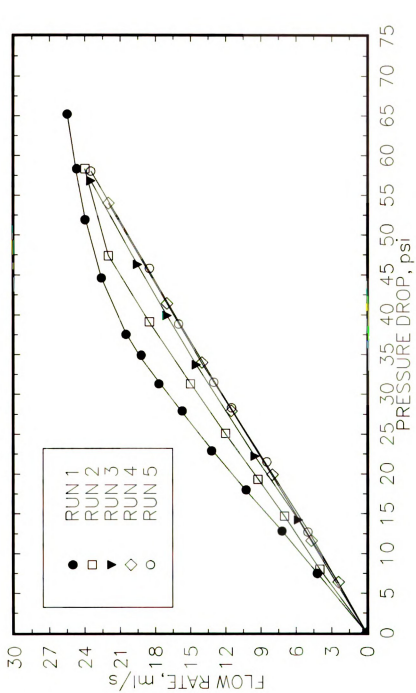

Figure 4.6b Hysteresis run (V_i = 0.56)

Table 4.2 Change in t_f for preform with initial volume fraction 0.46

Run #	t_f (cm)	V_f	K (Darcy)
1	0.2427	0.4583	6.88
2	0.2149	0.5063	5.36
3	0.2021	0.5383	4.61
4	0.1978	0.5500	4.35
5	0.1941	0.5604	4.13

$$V_{max} = 0.5604$$
$$V_{ini} = 0.4583$$
$$V_{max} - V_{ini} = 0.1121$$

Table 4.3 Change in t_f for preform with initial volume fraction 0.56

Run #	t_f (cm)	V_f	K (Darcy)
1	0.2365	0.5636	4.06
2	0.2187	0.6095	3.15
3	0.2102	0.6340	2.71
4	0.2078	0.6415	2.58
5	0.2074	0.6427	2.56

$$V_{max} = 0.6427$$
$$V_{ini} = 0.5636$$
$$V_{max} - V_{ini} = 0.0791$$

the calculations. The asymptotic value of fiber volume fraction (i.e., V_m) reached is different for both cases and is greater for a higher initial volume fraction. Sangani et al. [15] have mentioned that the maximum packing for a random preform is between 0.75 to 0.82. The fiber volume fractions obtained in Tables 4.2 and 4.3 seem to indicate that some more compaction can still be done, probably at higher pressure drops.

4.6 Compaction Model in through flow

Gutowski et al. [19] have obtained a relation between the effective stress carried by the fibers and the fiber volume fraction of a preform with aligned fibers. They modeled the fibers as beams with load acting at the center. The same approach has been used here to model the present compaction. Application of load on a fiber results in its deflection. As a result of this, the fibers in the upper layer come into contact with those in the lower layers. Restructuring of the mats is brought about due to movement of upper fibers into gaps present in the lower layer. This results in a net decrease in the thickness of the stack. The higher the load, the greater the restructuring, causing a greater decrease in stack thickness.

Each fiber span is modeled using the beam equations. The deflection is related to the change in thickness of the preform, which in turn is related to the fiber volume fraction. Figure 4.7 shows the fiber span schematically. $d\sigma$ represents the stress acting on the fiber to result in a deflection of dY. L is the span length. The beam equation relating load and deflection is given in [18] as -

$$dY = (d\sigma \cdot A) \frac{L^3}{48EI} \tag{4.5}$$

Here A is the area over which the stress acts, E is the Young's modulus and I is the moment of inertia, which for a beam with circular cross-section is given by

$$I = \frac{\pi}{64} d^4 \tag{4.6}$$

d is the diameter of the fiber, determined using a travelling microscope. E is a constant and is taken to be 76 GN/m^2 [20].

Using the condition that the deflection Y = 0 for $\sigma \leq \sigma_i$, equation (4.5) results in :

$$Y = (\sigma - \sigma_i) \frac{A}{48EI} L^3 \tag{4.7}$$

$$A = \pi L d \tag{4.8}$$

Substituting (4.8) in (4.7) yields

$$\begin{aligned} Y &= (\sigma - \sigma_i) \frac{\pi d}{48EI} L^4 \\ &= (\sigma - \sigma_i)\, s\, L^4 \end{aligned} \tag{4.9}$$

where the constant s is given by

$$s = \frac{\pi d}{48EI} \tag{4.10}$$

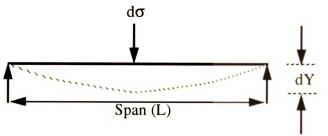

$$dY = (A\, d\sigma)\frac{L^3}{48EI}$$

Figure 4.7 Fiber Beam Analogy

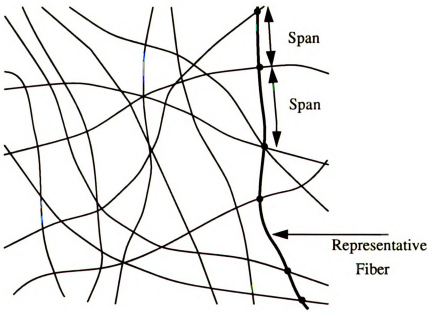

Figure 4.8 Fiber Span Schematic

Let t_i and t denote the initial thickness of preform and the thickness of preform at any time during compaction, respectively. The deflection Y can then be related to the thickness in the following manner :

$$Y = t_i - t \tag{4.11}$$

Combination of (4.9) and (4.11) yields

$$t_i - t = (\sigma - \sigma_i) s L^4 \tag{4.12}$$

Thickness may be related to the fiber volume fraction as shown in equation (2.2). Equations (2.2) and (4.12) result in equation (4.13), which relates the effective stress to the fiber volume fraction.

$$\frac{1}{V_i} - \frac{1}{V_f} = (\sigma - \sigma_i) \frac{s}{c} L^4 \tag{4.13}$$

Here V_i is the initial fiber volume fraction of the preform, corresponding to its thickness t_i.

Gutowski et al. [19] went ahead and assumed the span length L to be a linear function of thickness (or deflection), given by the following:

$$L = \beta (t - t_a) \tag{4.14}$$

Here t_a is the minimum possible thickness (corresponding to the maximum possible fiber volume fraction, V_a). β is a geometric factor. This resulted in the following expression:

$$\sigma = \frac{\pi}{64} \frac{E}{\alpha \beta^4} \frac{(\frac{1}{V_o} - \frac{1}{V_f})}{(\frac{1}{V_f} - \frac{1}{V_a})^4} \tag{4.15}$$

V_a is the maximum possible fiber volume fraction, V_o is the fiber volume fraction at which loading starts, β, the geometric factor is the ratio of span length to arch height and α is a geometric constant.

It should be pointed out again that the model proposed by Gutowski et al. [19], holds for aligned fibers only. Using the assumption mentioned in equation (4.14), the authors have converted the span length to a function of fiber volume fraction, with the addition of two parameters V_a and β. However, the present set-up does not consist of aligned fibers. Since the present fibers are randomly arranged, they cross each other at many points throughout the length. Hence, the entire fiber cannot be considered as the span length. The tiny portion of the fiber in between two contact points is the span length (see Figure 4.8), the value of which can be experimentally measured. Calculated σ and V_f may be fitted with equation (4.13) to yield the computed span length. This, when compared with the experimental span length, provides a method for testing the proposed model. Hence, the present analysis does not use equation (4.14), thereby retaining L as a function of V_i and V_f only.

Later modifications of the original model proposed in [19] resulted from the assumption that the arched fiber could be represented by boxes of equal height and width. Such an assumption can not be used for randomly arranged, continuous fibers. Hence, the later models have not been considered for the present use.

4.7 Preliminary testing of present model

As pointed out in section 4.6, the parameter L in equation (4.13) may be fitted to the compaction data and this can be compared with the experimental span length. To do so, fiber volume fractions were determined at various pressure drops using equations (1.2), (2.2) and (3.5). The parameter (σ-σ_i) was plotted against $1/V_f$. This is shown in Figure 4.9. Different slopes were obtained for different initial fiber volume fractions. This is expected since the value of 'c' changes with V_i. From the slopes, L was determined for each of the cases. These are shown in Table 4.4. It is seen that L is of the order of 1 mm. This seems reasonable, since actual L (i.e., distance between two contact points) is also of the same order.

Table 4.4 Preliminary testing of model

Initial V_f	L (mm)	y-int (Figure 4.11) (psi)	actual σ_i (psi)
0.46	1.18	17.5	17.1
0.51	1.21	20	20
0.56	1.20	25	22.9

Since L obtained was almost the same for all cases tried, a plot of (σ-σ_i) vs ($1/V_i$-$1/V_f$) was made (Figure 4.10). As expected it resulted in a set of lines passing through the origin and having different slopes. A plot of σ vs ($1/V_i$ - $1/V_f$) is shown in Figure 4.11. This plot consists of straight lines with y-intercept close to the actual σ_i values, as shown in Table 4.4. Thus, agreement between the experimental data and equation (4.13)

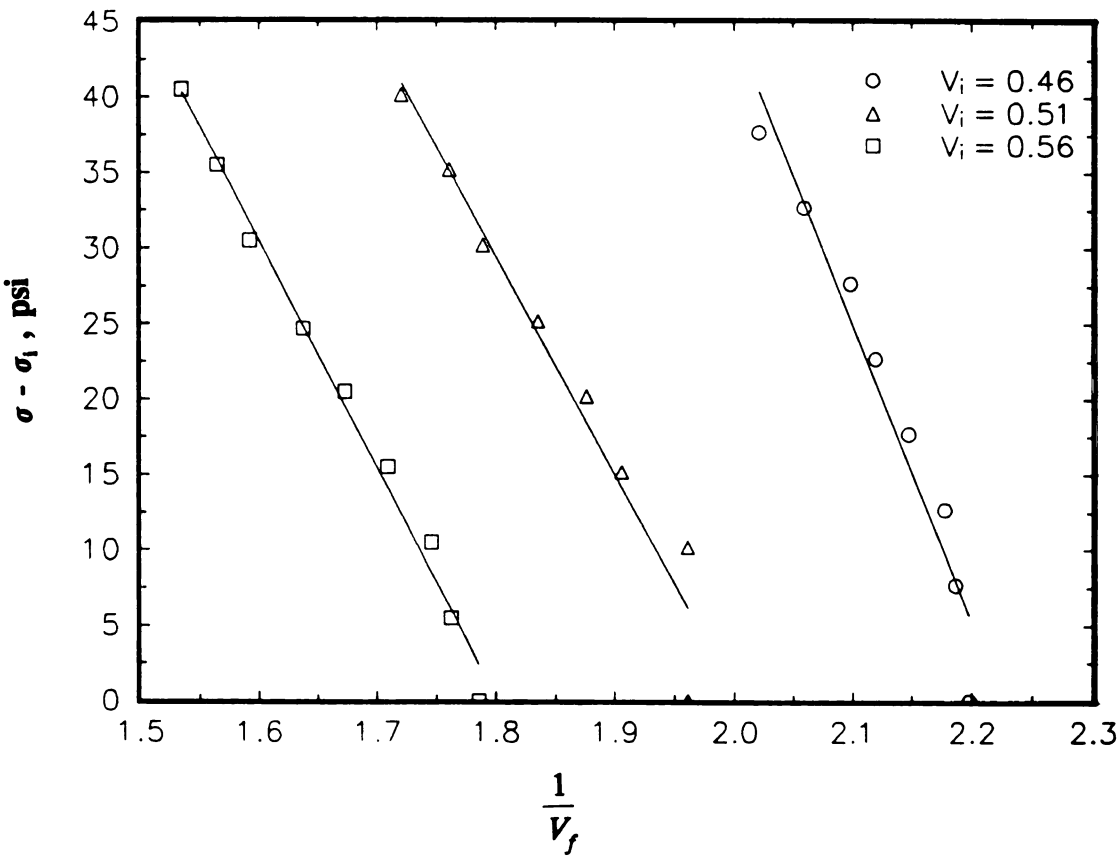

Figure 4.9 Determination of L

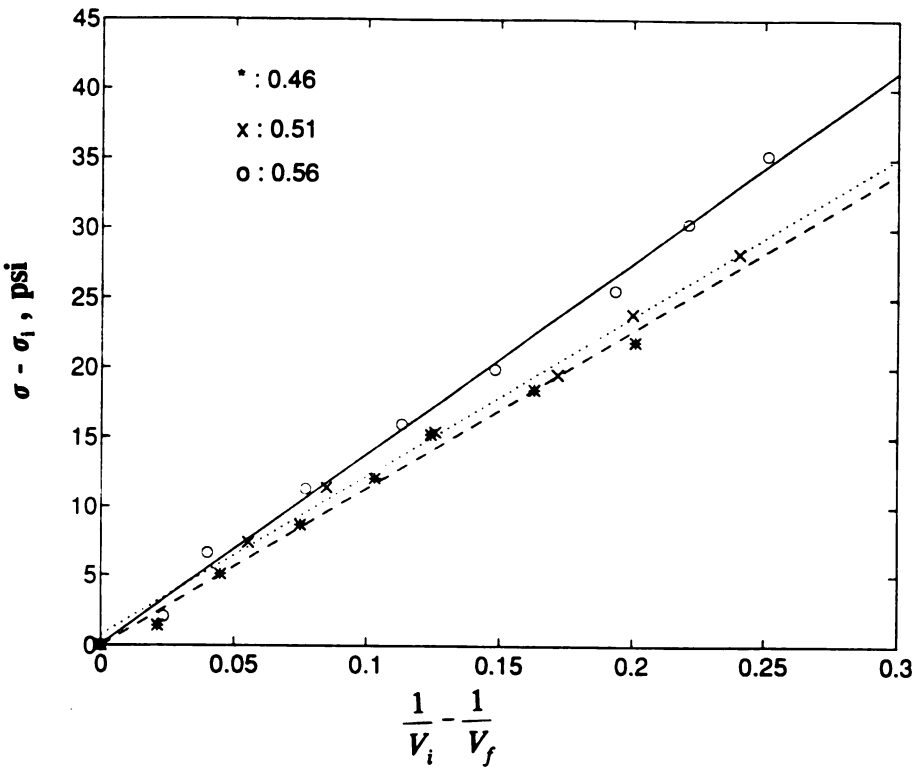

Figure 4.10 Preliminary testing of model

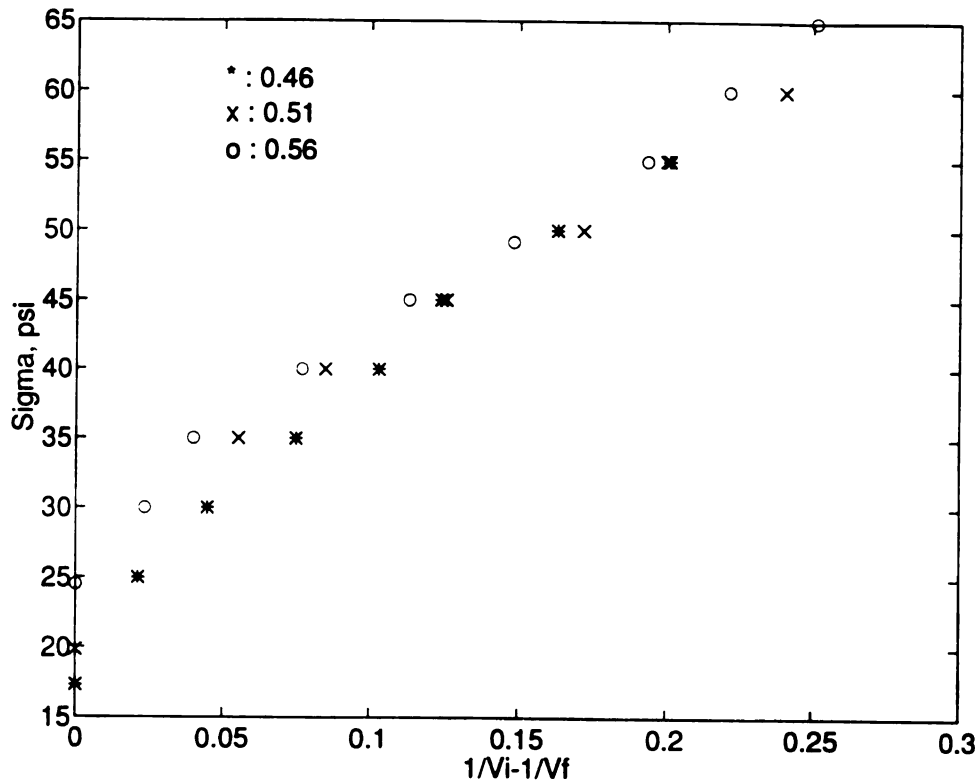

Figure 4.11 Preliminary testing of model - σ_i determination

is preliminarily confirmed. Complete correctness can, of course, be verified only by the prediction of the nonlinear portion of the pressure drop - flow rate curve. This is discussed later.

Effective stress studies were carried out for runs with fluids of higher viscosities, as before. The σ - V_f curve obtained is shown in Figure 4.12. It can be seen that a different trend is shown with the more viscous fluid. σ changes very little initially, but tends to rise quickly at higher volume fractions. With the lower viscosity fluid, the effective stress rises very fast in the beginning, but slows down toward the end. The shape of the curves (with the higher viscosity fluid), seems to indicate that Gutowski's model [19] would fit these curves well (note the similarity between these curves and Figure 1.2). However, the best possible fits for these curves are obtained with seemingly absurd values of fitting constants (eg., the maximum fiber volume fraction V_a, comes out to be about 12 !). Though Gutowski's fit could not be successfully accomplished, it is possible that the σ - V_f model proposed in [19] holds only for high values of applied load ($\sigma \sim 400 - 500$ psi). Hence, experiments with very viscous fluids might yield curves more similar to those shown in Figure 1.2.

4.8 Pressure drop - flow rate curve prediction

This section is based on the results obtained in Chapters 3 and 4. The objective here is to predict the entire pressure drop - flow rate curve, given the initial fiber volume fraction and load used to prepare the preform. Also needed are the dimensions and mass

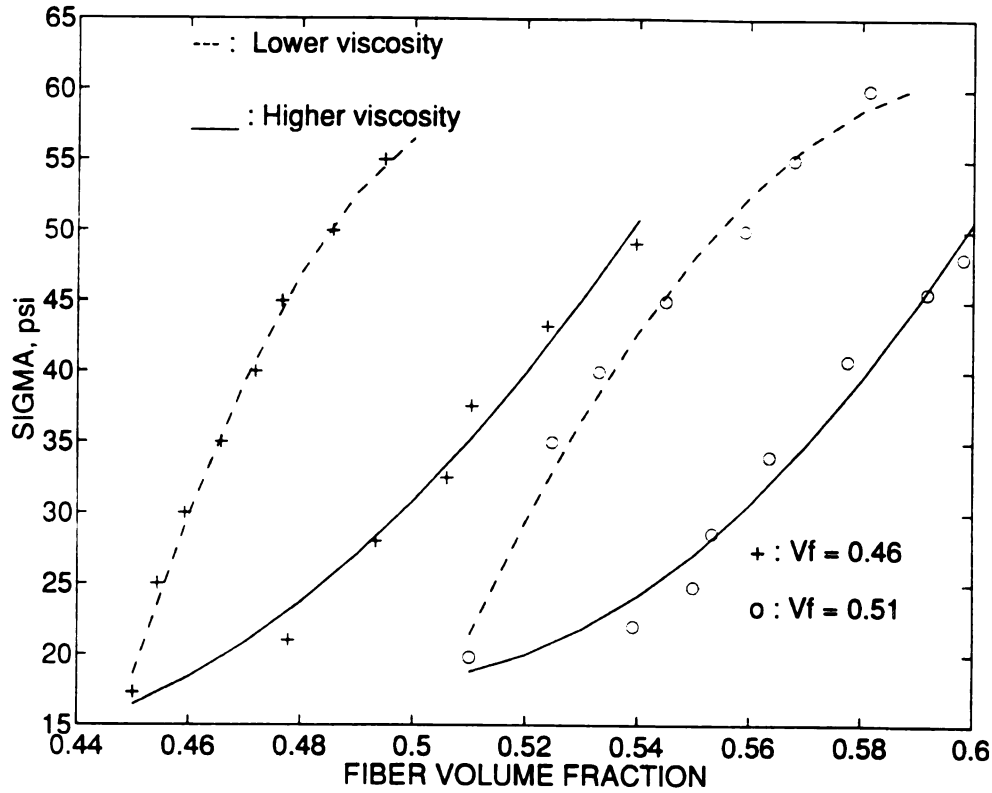

Figure 4.12 Effect of fluid viscosity on effective stress

of the preform, diameter of the fibers and viscosity of the fluid used. Following are the steps involved :

(1) Using equation (3.5) and the known initial fiber volume fraction, determine the Darcy permeability (K_{zz}).

(2) Calculate critical pressure drop (ΔP_c) from the preforming load, by dividing load by the platen area.

(3) Determine Q_c from Darcy's law (equation 1.2) by substituting K_{zz} and ΔP_c obtained from steps (1) and (2).

(4) Join origin and the point (ΔP_c,Q_c). This yields the linear portion of the plot.

(5) Choose a pressure drop greater than ΔP_c. This is also the effective stress σ. Use equation (4.13) to determine V_f.

(6) Using V_f from above, determine permeability K_{zz} and thickness t_f [equations (2.2) and (3.5)].

(7) Compute the flow rate using Darcy's law (equation 1.2).

(8) Select a higher pressure drop and repeat the process.

Steps 1 through 8 will result in the development of the entire pressure drop - flow rate curve.

It should be mentioned that this set of working steps will be applicable only in the pressure drop range tested (0 - 70 psi). A higher range might require some modifications to the constants used in some of the equations above. Hence, it would be advisable to maintain pressure drop within the said range.

Using the steps outlined above, predictions were made and compared with the data. Results of this are shown in Figure 4.13. A slight discontinuity can be seen in all the three predicted curves. This is because of the error involved in calculating the critical flow rate from the critical pressure drop. A value of 1.2 mm for span length L has been used in equation (4.13), for all the three cases.

A point which needs to be brought out is that, till date, no results for predictions of the non-linear region have been proposed. The maximum error involved in using equation (4.13) is about 8 %. Thus, equations (2.2), (3.5) and (4.13) provide a simple but effective way of predicting the entire pressure drop - flow rate profile, given the preforming load, preform dimensions and fluid viscosity.

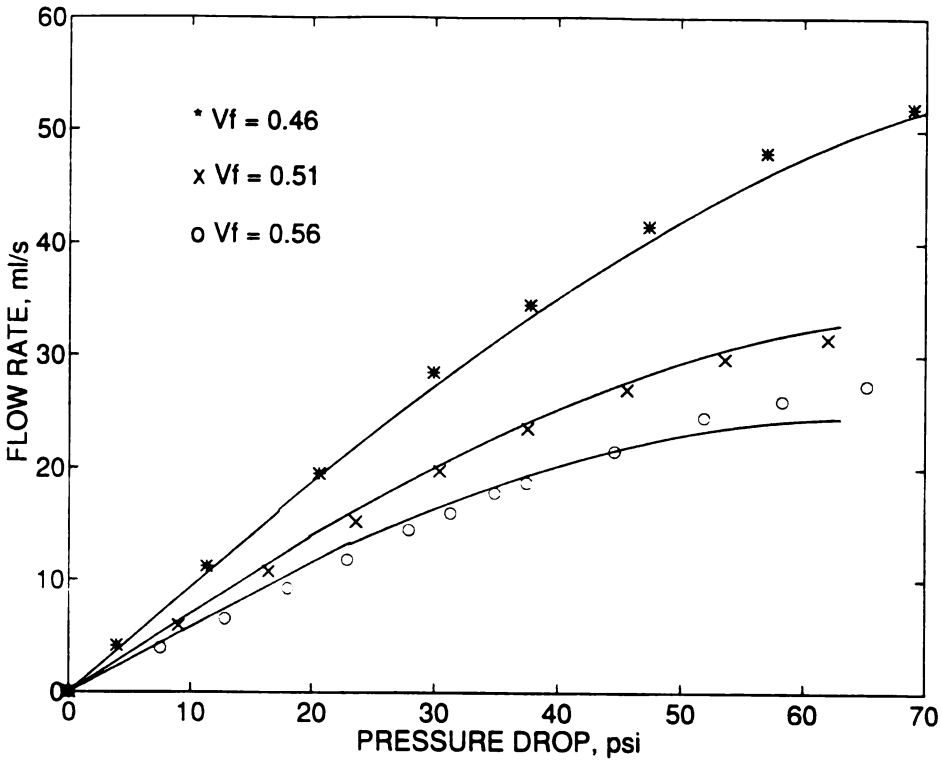

Figure 4.13 Model prediction

Chapter 5 Conclusions and Recommendations

5.1 Conclusions

The following conclusions can be drawn from the present study -

(1)The transverse permeability of continuous strand, random glass fiber mats to mixtures of glycerol and water have been measured. Permeability is found to vary from 20 Darcy to 3.6 Darcy for an initial fiber volume fraction range of 0.4 to 0.6. The range of permeability values and the trend observed in the pressure drop - flow rate curves (i.e., excess pressure drop at higher flow rates), indicate that the permeation cell designed for experimental measurements is free from channeling effects.

(2)The wetting characteristics of the fluid used have been compared with that of Derakane 411-C50 and Corn oil, since the latter has been used by many workers as a resin for permeability studies. The present fluid has been found to have a contact angle close to Derakane, leading to the inference that the fiber-fluid interaction is similar in both systems, i.e., glass - Derakane and glass - glycerol+water solution.

(3)Permeability drops with increasing fiber volume fraction, as expected. The drop is more obvious at the lower end of fractions tested (~ 40 %) than the more densely packed fractions (~55-60 %). A relation has been proposed (equation 3.5) to predict the permeability from the fiber volume fraction. The proposed equation predicts a maximum packing (V_m) of 89 %, at which the permeability drops to zero. Equation (3.5) fits the

whole range of fiber volume fractions studied. The Karman - Cozeny equation and its modification [7] are found to be inadequate here, as in other preforms involving continuous fibers.

(4)The point at which the onset of compaction sets in has been shown to have a physical significance. The pressure drop at this point (critical pressure drop) increases with increase in initial fiber volume fraction. Further, it is equal to the pressure exerted by mechanical means on the preform, during its preparation. This has been found to be true for various initial fiber volume fractions.

(5)Compaction of preforms due to flow has also been studied in the present work. Compaction is more clearly seen for preforms with lower initial fiber volume fractions. The reason for this is that the more densely packed preforms ($V_f \sim 60$ %) are already in a very compressed state, leaving little scope for further compaction. A method has been proposed to determine the fiber volume fraction of the preform in the compacted state. This method uses a model (equation 4.13) developed in the present study. The model applies structural beam equations to a fiber and relates the deflection to change in preform thickness. The fluid pressure drop is considered as the load acting on the beam (fiber). The model contains a parameter L (span length), which can be experimentally measured. The effective stress - fiber volume fraction behavior is quite different from that shown in [7], wherein the source of effective stress carried by the fibers is the mechanical compression of the preform and not continuous flow of fluid through the preform.

(6)The effect of fluid viscosity on compaction has been studied. At the same pressure

drops, a more viscous fluid compacts the preform to a larger extent. The permeability in the linear region is, however, unaffected by the viscosity. The preforms with higher volume fractions ($\sim$50 %) are seen to be minimally affected by the change in viscosity of the fluid. It would, therefore, be advantageous to work in the higher fraction range to counter the effect of increasing viscosity (eg., during curing). Effective stress on fibers, caused by flow of higher viscosity fluid increases gradually at lower fiber volume fractions, but rises sharply at higher volume fractions. This trend is similar to that observed in [7], unlike in the case using less viscous fluid. This implies that the model proposed in [7], holds for high degrees of applied loads ($\sigma \sim$ 400 - 500 psi) only.

(7)Hysteresis studies have been carried out on the preform. The effect of changing thickness (due to flow compaction) has been incorporated into the permeability-measurement technique. With every subsequent run, the linear region is observed to become more pronounced till finally most of the pressure drop - flow rate curve becomes a straight line. The asymptotic value of fiber volume fraction (i.e., V_m) is observed to be greater for a higher initial fiber volume fraction. Inequality of this value for different preforms, indicates that still more compaction is possible at higher flow rates.

(8)A working set of equations for predicting the entire pressure drop - flow rate profile has been developed. Results using these show an excellent agreement with experimental data. The maximum error involved in the present predictions is about 8 %.

5.2 Scope of future work

(1)Various preforms employing the same type of fiber mats but at varying fiber volume fractions, have been used in the present study. Preforms consisting of different kinds of fibers need to be used, too. This can provide an additional parameter in the study i.e., stacking sequence and its effect on permeability and compaction.

(2)Though the permeation cell is properly designed for the present study, it would be useful to develop a similar cell with a few modifications. An arrangement to simultaneously measure the fiber volume fraction during compaction, would be a tremendous asset in verifying any model proposed in the study (including the model equations proposed in the present work). Design modification should also include a channeling - proof method to use preforms of varying thicknesses (using spacers).

(3)Flow visualization experiments can be carried out to understand the preform compaction process better. The cell design would have to be altered to accommodate this objective.

(4)More work needs to be done to explain the true effect of viscosity of fluid on the compaction process. The present work in this aspect, only provides a starting point for future study. It would also be beneficial to model this effect mathematically.

APPENDICES

APPENDIX 1

Wicking Experiment

Following is the description of the wicking experiment carried out to determine the fluid-fiber interactions. The method has been taken from Chwastiak [14].

Figure A.1.1 shows the loading of glass fibers into a teflon tube of internal diameter 2.38 mm. About 40 - 50 strands of the fibers are pulled into the tube using a string, resulting in a fiber volume fraction in the tube of 0.5. About 2 mm of the fiber is left protruding beyond the top surface of the tube. The tube is then suspended from a Sartorius analytical balance, with its lower end just dipping into the fluid. This assembly is then placed on a lab jack to facilitate the easy movement of the beaker containing the wicking liquid. This is illustrated in Figure A.1.2.

The measurement consists of recording the increase in mass of the tube as a function of time. This process is continued till a constant mass is reached and no more wicking takes place. Neglecting the inertial forces, the expression proposed in [14] is of the form :

$$\Delta\gamma = \frac{128(1-\epsilon)^2 H^2 \rho_f \mu \alpha}{K^2 \epsilon^3 V_T W_f d_f \rho_l^2} \left(\frac{m^2}{t}\right) + \frac{g \rho_f d_f H}{4 W_f} (m) \qquad \text{(A.1.1)}$$

Here $\Delta\gamma$ is the difference in surface free energy between a unit area of dry surface and a unit area of wetted surface. m is the mass of wicking liquid at time t. The parameters employed in the above equation are described in Table A.1.1. Thus using equation

(A.1.1), $\Delta\gamma$ for all the three liquids may be determined.

The equlibrium contact angle (θ) between the fiber and the liquid surface can be correlated to the surface tension of the liquid (γ_l), by using the following expression -

$$Cos\theta = \frac{\Delta\gamma}{\gamma_l} \qquad \text{(A.1.2)}$$

Table A.1.1 Parameters used in equation (A.1.1)

Parameter	Description	Value	Units
ϵ	Porosity in fiber bundle	0.5	-
H	Height of fiber bundle	varying	cm
ρ_f	Density of fiber	2.56	gm/cm^3
μ	Viscosity of liquid	varying	cp
α	Slope of m vs t on a log-log plot	0.5	-
m	Mass of wicking liquid at any time t	varying	gm
K_h	Hydraulic constant	4	-
V_T	Total volume occupied by fiber bundle	varying	cm^3
W_f	Weight of fiber bundle	varying	gm
d_f	Filament diameter	30	microns
ρ_l	Density of liquid	varying	gm/cm^3
g	Gravitational constant	980	cm/s^2
t	Time	varying	s

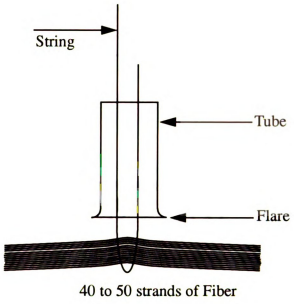

Figure A.1.1 Loading of Fiber into a tube

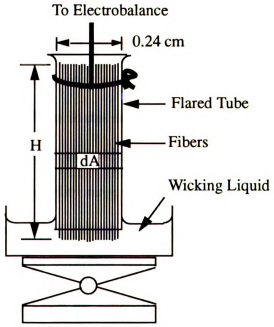

Figure A.1.2 Wicking of liquid into fiber bundle

APPENDIX 2

Older Design Permeability

Four different initial fiber volume fractions have been tested with the older assembly design - 21, 39, 48 and 64%. Figure A.2.1 presents the results of superficial velocity times fluid viscosity against the pressure gradient, for different fiber volume fractions. Pressure gradient is plotted here since the thickness of the preform varies for each of the curves shown. Thus, the slopes of the linear region represent the permeabilities. Since very high pressures were not employed in this case, the nonlinearity is not pronounced. However, slight deviations for the cases of 39% and 64% fiber volume fraction are shown. The deviation in the latter case is not as sharp as in the former, since it is believed that most of the packing has already been achieved at the beginning of the process itself, not leaving much scope for further compaction. As shown earlier (Figure 2.4), the permeabilities in this case are found to be 4 - 8 times higher than those obtained with the new preform assembly design. This figure provides a valuable piece of information - if the permeability range observed by any other worker (using the same type of fiber and the same fiber volume fraction range) is similar to that seen by the older assembly design, it can be concluded that channeling effects are being exhibited and attempts must be made to prevent the same, in order to cause good wet-out of the composite part.

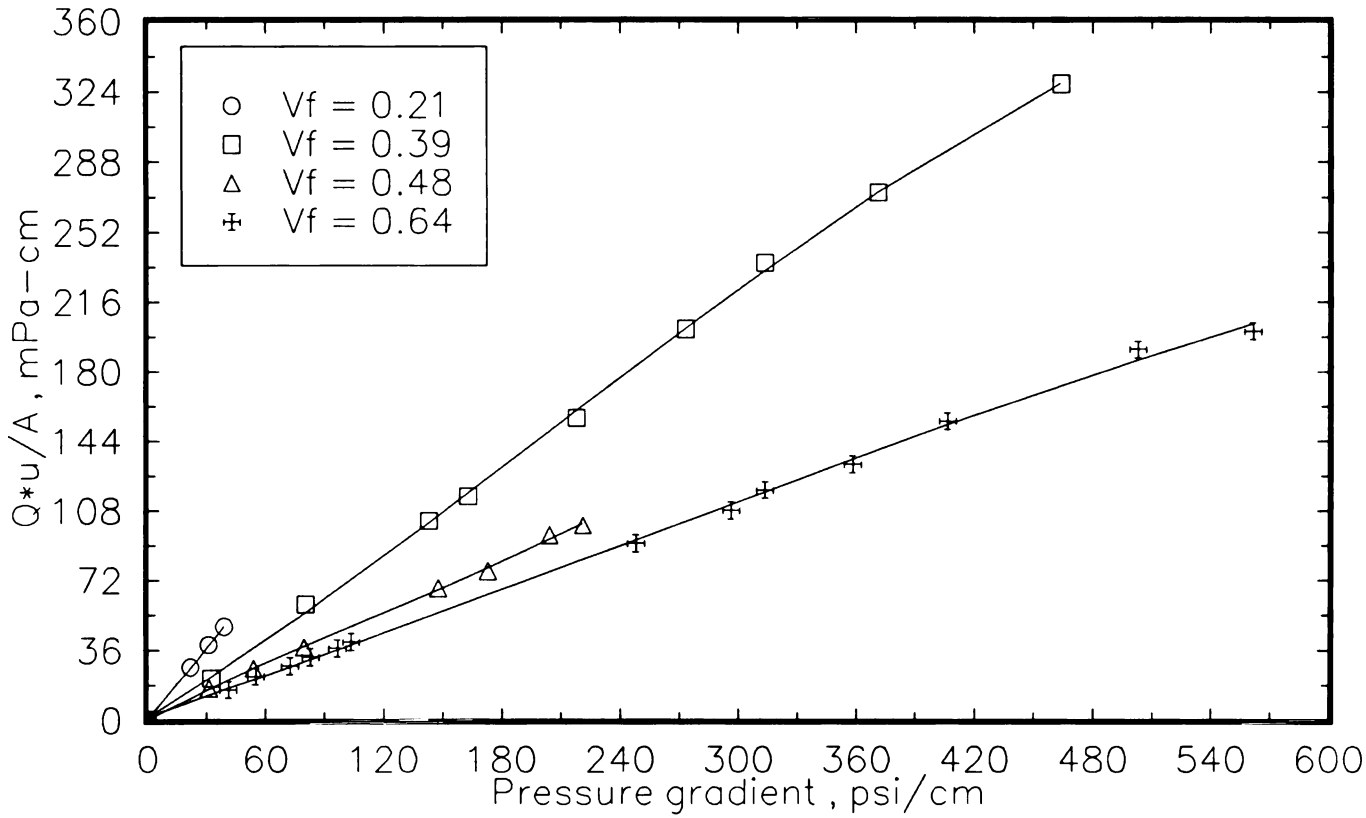

Figure A.2.1 Pressure drop - Flow rate data (old design)

BIBLIOGRAPHY

BIBLIOGRAPHY

(1) Knoblach, G.M., *Encyclopedia of Composite Materials*, McGraw-Hill, 1991.

(2) Gauvin, R. Chibani, M. and Lafontaine, P., "*The Modeling of Pressure Distribution in Resin Transfer Molding*", J. Reinf. Plastics Compos., **6**, Oct. 1987, 367-377.

(3) Adams, K.L. and Rebenfeld, L., "*In-plane Flow of Fluids in Fabrics : Structure / Flow Characterization*", Textile Res. J., **57**, 1987, 647-654.

(4) Molnar, J.A., Trevino, L. and Lee, L.J., "*Liquid Flow in Molds with Prelocated Fiber Mats*", Polym. Compos., **10**(6), Dec. 1989, 414-423.

(5) Kim, Y.R. and McCarthy, S.P., "Compressi*bility and Relaxation of Fiber Reinforcements during Composite Processing*", Polym. Compos., **12**(1), Feb. 1991, 13-19.

(6) Salem, A.J. and Parnas,. R S., "*The Unidirectional and Radial In-plane flow of fluids through Woven Composite Reinforcements*", Proc. Am. Soc. for Comp. Sixth Techn. Conf., Oct. 7-9, 1991, 1012-1021.

(7) Gutowski, T.G., Cai, Z., Bauer, S., Boucher, D., Kingery, J. and Wineman, S., "*Consolidation Experiments for Laminate Composites*", J. Compos. Mater., **21**, July 1987, 650-669.

(8) Skartsis, L., Khomami, B. and Kardos, J.L., "*Resin Flow through Fiber Beds during Composite Manufacturing Processes- Part II: Numerical and Experimental Studies of Newtonian flow through Ideal and actual Fiber Beds*", Polym. Eng. Sci., **32**(4), Feb. 1992, 231-239.

(9) Morse, C.T., Ochoa, O.O., Barron, J.H. and Barron, D.L., "*Optimization of SRIM Automotive Bumper Beams through Permeability and Wet-out characterization*", Preprint of Paper presented at the 8th Annual ASM/ESD Adv. Compos. Conf., Chicago, Nov. 1992..

(10) Trevino, L., Rupel, K., Young, W.B., Liou, M.J. and Lee, L.J., "*Analysis of Resin Injection Molding in Molds with Preplaced Fiber Mats- I: Permeability and Compressibility Measurements*", Polym. Compos., **12**(1), Feb. 1991, 20-29.

(11) Berdichevsky, A.L. and Cai, Z., "*Preform Permeability Predictions by Self-Consistent Method and Finite Element Simulation*", Polym. Compos., **14**(2), April 1993, 132-143.

(12) Gutowski, T.G., Kingery, J. and Boucher, D., "Experiments in *Composites Consolidation : Fiber Deformation*", Proc. SPE ANTEC, Boston, May 1986.

(13) Lam, R.C. and Kardos, J.L., "*The permeability and Compressibility of Aligned and Cross-plied Carbon Fiber Beds during procesing of Composites*", Polym. Eng. Sci., 31(14), July 1991, 1064 -1070.

(14) Chwastiak, S., "A Wicking *method for measuring Wetting Properties of Carbon Yarns*", J. Colloid Interface Sci., **42**(2), Feb. 1973, 298-309.

(15) Sangani, A.S. and Yao, C., "*Transport Processes in Random Arrays of Cylinders - II - Viscous flow*", Phys. Fluids, **31**(9), Sept. 1988, 2435-2444.

(16) Berdichevsky, A.L. and Cai, Z., "*Prediction of Permeability of Fibrous Media using Self-consistent method*", Symposium on Science & Innovation in Polym. Compos. Proc., M.I.T., July 1992.

(17) Kim, Y.R., McCarthy, S.P. and Fanucci, J.P., "*Flow Behavior through Fiber Reinforcements during Composite Processing*", SPE Regional Technical Conf. on Advancements in Materials for Polymer Composites and Special Topics, Oct. 16-18, 119-143.

(18) Willems, N., *Strength of Materials*, McGraw Hill, New York, 1981.

(19) Gutowski, T.G., "*A Resin flow/Fiber deformation model for Composites*", SAMPE Quart., **16**(4), July 1985, 58-64.

(20) Hull, D., *An introduction to Composite Materials*, New York: Cambridge University Press, 1981.

(21) Gutowski, T.G., Morigaki, T. and Cai, Z., "*The consolidation of Laminate Composites*", J.Compos. Mater., **21**(2), Feb. 1987, 172-188.

(22) Kim, Y.R., McCarthy, S.P., Fanucci, J.P., Nolet, S.C. and Koppernaes, C., "*Resin Flow through Fiber Reinforcements during Composite Processing*", SAMPE Quart., April 1991, 16-22.

(23) Williams, J.G., Morris, C.E.M. and Ennis, B.C., "*Liquid Flow Through Aligned Fiber Beds*", Polym. Eng. Sci., **14**(6), 1974, 413-419.

(24) Adams, K.L. and Rebenfeld, L., "*Permeability Characteristics of Multilayer Fiber*

Reinforcements. Part I: Experimental Observations", Polym. Compos., **12**(30), June 1991, 179-190.

(25) Vossoughi, S. and Seyer, F.A., "*Pressure Drop for Flow of Polymer Solution in a Model Porous Medium*", Can. J. Chem. Eng., **52**, Oct. 1974, 666-669.

(26) West, B.P.V., Pipes, R.B. and Advani, S.G., "Consolidation *of Commingled Thermoplastic Fabrics*", Poylm. Compos., **12**(6), Dec. 1991, 420-427.

(27) Perry, R.H. and Chiton, C.H., *Chemical Engineers' Handbook*, 5th ed., New York: McGraw-Hill Book Company, 1973.

(28) Parnas, R.S. and Phelan, F.R.Jr., "*The Effect of Heterogeneous Porous Media on Mold Filling in Resin Transfer Molding*", SAMPE Quart., Jan. 1991, 53-60.

(29) Reid, R.C. and Sherwood, T.K., *The Properties of Gases and Liquids*, 2nd ed., McGraw-Hill Book Company.

(30) Skartsis, L., Kardos, J.L. and Khomami, B., "*Resin Flow Through Fiber Beds During Composite Manufacturing Processes. Part I: Review of Newtonian Flow Through Fiber Beds*", Polym. Eng. Sci., **32**(4), Feb. 1992, 221-230.

(31) *Handbook of Chemistry and Physics,* 73rd ed., The Chemical Rubber Company, Cleveland, Ohio, 1992-93.